Tectonophysics 819 (2021) 229078

Contents lists available at ScienceDirect

Tectonophysics

journal homepage: www.elsevier.com/locate/tecto

From downbuilding to contractional reactivation of salt-sediment systems: Insights from analog modeling

P. Santolaria [a,*], P. Granado [a], N. Carrera [a], C.L. Schneider [b], O. Ferrer [a], M. Snidero [a], P. Strauss [c], K. Pelz [c], E. Roca [a], J.A. Muñoz [a]

[a] Institut de Recerca Geomodels, Departament de Dinàmica de la Terra i de l'Oceà, Universitat de Barcelona, Martí i Franquès s/n 08028, Barcelona, Spain
[b] ConocoPhillips, Houston, TX, USA
[c] OMV Exploration and Production GmbH, Trabrennstrasse 6-8, 1020 Vienna, Austria

ARTICLE INFO

Keywords:
Salt-sediment interaction
Isolated-minibasin provinces
Thrust wedge
Downbuilding
Welding
Fault weld

ABSTRACT

This work studies salt-detached fold-and-thrust belts involving minibasins by means of physical analogue modeling. The experimental set up consist of a series of minibasins and diapirs built by downbuilding into a regular polygonal framework. The minibasins-diapir framework were then submitted to contraction, and for some examples accompanied by different rates of syncontractional sedimentation. We aimed at evaluating the influence of an initial salt basin geometry (i.e. equal thickness vs. along-strike tapered) on the development of the salt-sediment system, and how this influences the geometries and kinematics of fold-and-thrust belts. We also tested how these are influenced by different syncontractional sedimentation rates. Results show that major differences on the early salt structures occur during downbuilding as a result of original salt budget (i.e. from pillows to diapirs), with a positive correlation between amount of original salt and salt structure development. Initial contractional deformation is localized on the weaker salt bodies, favoring salt extrusion. Shortening is then transferred forwards once vertical salt feeders are welded (i.e. secondary welds), while basal (primary) welds are sheared, rolled or delaminated. Changes on structural styles occur abruptly along-strike as controlled by degree of development of the precontractional salt structures. Relatively low syncontractional sedimentation rate delays forward propagation of deformation and promotes minibasins tilting. With larger sedimentation rates, a thicker cover inhibits minibasins deformation and secondary welding and, promotes a more coherent mechanical beam detached on the basal weld. Our modeling is compared to natural fold-and-thrust belts such as the Zagros and the European Alps.

1. Introduction

The structural styles observed across many fold-and-thrust belts do not comply with the classical *Rocky Mountain style* thrust sheets involving a sedimentary cover of regionally even stratigraphic thickness (i.e. *layer-cake*). In fact, many salt-detached fold-and-thrust belts such as the easternmost Fars of the Iranian Zagros (e.g. Callot et al., 2012; Snidero et al., 2019), the Northern Calcareous Alps of Austria (e.g. Granado et al., 2019; Strauss et al., 2020), the Provençal Western Alps of France (Graham et al., 2012) developed from the inversion and incorporation of rifted margin sedimentary sequences involving early (i.e. precontractional) salt structures, such as minibasins flanked by diapirs. These structures have been termed *isolated-minibasin provinces* (Duffy et al., 2021), and involve minibasins formed by downbuilding completely surrounded by diapirs and conforming polygonal or sub-circular arrays (Rowan and Vendeville, 2006; Harrison and Jackson, 2014; Duffy et al., 2018; Jackson and Hudec, 2017; Dooley et al., 2019; Strauss et al., 2020). Since the precontractional array of minibasins and salt structures is structurally complicated per se, the structural styles developed upon orogenic convergence become complicated further and difficult to ascertain and understand in 3D (Graham et al., 2012; Kergaravat et al., 2016; Granado et al., 2019). Cross-section and 3D model construction remain therefore challenging, and especially onshore, where seismic data is generally sparse and of low-quality (Legeay et al., 2019; Snidero et al., 2019). An important driver for researching these systems relates to their economic relevance as they include voluminous sediment accumulations, host key natural resources, and are a rich archive of global environmental and climate change.

* Corresponding author at: Institut de Recerca Geomodels, Departament de Ciències de la Terra i de l'Oceà, C/Martí i Franquès s/n 08028, Barcelona, Spain.
E-mail address: p.santolaria.otin@ub.edu (P. Santolaria).

https://doi.org/10.1016/j.tecto.2021.229078
Received 12 December 2020; Received in revised form 26 August 2021; Accepted 20 September 2021
Available online 25 September 2021

To overcome these challenges and reduce uncertainty for decision making, we have designed an experimental sandbox modeling program to unravel how contractional reactivation of minibasins and flanking salt diapirs impact thrust wedge geometries and kinematics. In our experimental approach we have used a relatively simple scenario that allowed focusing on a series of topics which we consider fundamental: i) what is the impact of the basal salt architecture in the development of the salt-sediment system during downbuilding? ii) how do the resulting geometries control the structural styles and kinematics upon shortening, and how these relate to the critical taper of thrust wedges? iii) and how does syncontractional sedimentation impacts the deformation of the salt-sediment system during contraction? Our experimental results are presented, discussed, and compared to the Fars salient of Iran and the Northern Calcareous Alps of Austria.

2. Analog modeling

2.1. Rationale

In previous modeling works involving shortened isolated-minibasin provinces, modelers used an uneven distribution of minibasins and surrounding salt diapirs (Rowan and Vendeville, 2006; Ferrer, 2012; Callot et al., 2016; Dooley et al., 2019; Duffy et al., 2021) We have adopted a different approach by using a regular minibasin framework (Fig. 1a). Our closest natural analog, which served as inspiration for the experimental program, is the Fars Province of the Zagros Simply Folded belt of Iran. The designed experimental pattern results from the simplification of the structural grain found in the eastern Fars province, where extruded and buried salt diapirs are likely connected at depth through a network of salt ridges. Besides, by choosing such regular pattern we intend to avoid interpreting uncertainties related to an initially random distribution of minibasins. In particular, we investigate the influence of the salt basin geometry. To do this, we carried out and compared one model using a horizontal and constant thickness basal model salt, and other with an along-strike tapered-thickness model salt (Fig. 1). Such oblique-to-contraction distribution of salt stands as one of the main features not only in the Fars province (Bahroudi and Koyi, 2003; Bahroudi and Talbot, 2003) but also in the southern Pyrenees (Muñoz et al., 2013) and the Jura Mountains (Sommaruga, 1999) among others.

As a second step in the experimental program, we also examine the impact of syncontractional sedimentation rate on the contraction of isolated-minibasin provinces. Being aware of the impact of erosion in natural and analog fold-and-thrust belts (e.g. Konstantinovskaya and Malavieille, 2011), we again invoke the Fars province to justify the use of just syncontractional sedimentation. In the Fars province, continuous sedimentation filled the Fars foreland from Campanian times (Snidero et al., 2020) where erosion localized in the crest of growing salt bodies and anticlines.

The experimental program was designed to analyze different scenarios during the same experiment. Such configuration should allow studying the geometrical and kinematical evolution from hinterland to foreland (i.e. closer to or away from the moving backstop wall) but also along the strike of thrust wedges involving such different domains. We

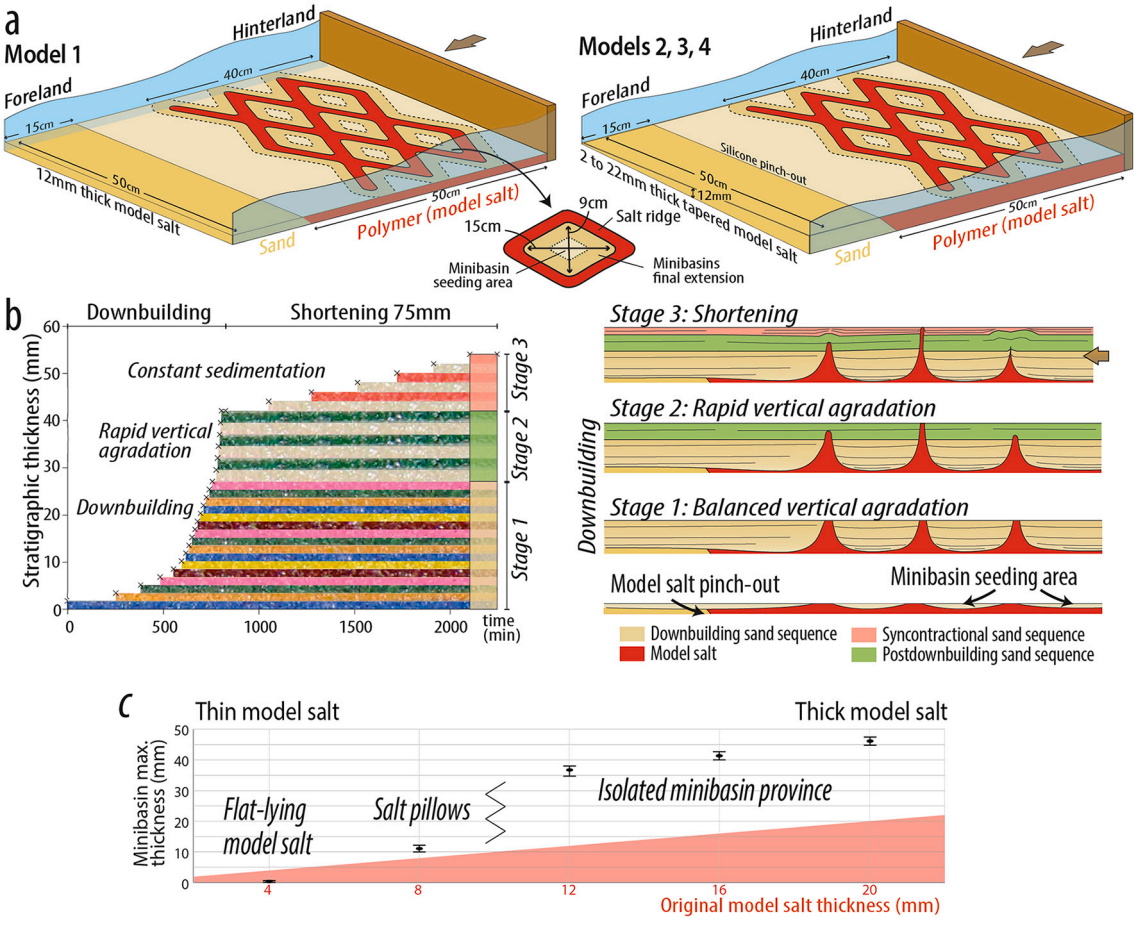

Fig. 1. a) Set up for Model 1 and Models 2, 3 and 4. Note the geometry of the model salt layer and the location and pattern of minibasins and salt ridges. b) Left, stratigraphic thickness vs. time during downbuilding (Stages 1 and 2) and shortening (Stage 3) and right, sketched evolution of an idealized model showing stages 1 to 3. c) Graph depicting the relation between maximum minibasins thicknesses registered at the end of stage 1 (Black circles) vs. the original model salt in red. (For interpretation of the references to colour in this figure legend, the reader is referred to the web version of this article.)

also consider that other boundary conditions may be important to test, such as an oblique frontal buttress, or other (regular) angular relationships within the salt network, or syncontractional erosion; however, including these were considered out of the focus of this work.

2.2. Analog material and scaling parameters

The models were constructed using materials suitable to carry out simulations of upper crustal deformation (see Weijermars and Schmeling, 1986; Schellart, 2000; Dell'Ertole and Schellart, 2013 for reviews). For modeling non-salt rheology, we used dry well-sorted quartz sand with an average grain size of 199 μm, a mean coefficient of friction (φ) of 0.69 and a cohesive strength of 55 Pa (Ferrer et al., 2017), and an average angle of internal friction (ø) of ~34° and a bulk density of 1500 kg/m^3. Lohrmann et al. (2003) and Adam et al. (2005) demonstrated that sand displays an elastic/frictional plastic behavior with transient strain hardening prior to transition to stable sliding. According to these authors, the behavior of dry quartz sand departs from the classically accepted Mohr-Coulomb rheology (e.g., Hubbert, 1951), but remains a good mechanical analog for modeling the brittle behavior of upper crustal rocks.

As an analog of salt in nature, a transparent high-viscosity polydimethylsiloxane polymer (Rhodosil GUM FB) from Bluestar Silicones was used (see Dell'Ertole and Schellart, 2013). At the low strain rates used in sandbox model experiments, this polymer behaves as a nearly-Newtonian fluid with low yield strength (e.g., Weijermars and Schmeling, 1986; Dell'Ertole and Schellart, 2013), simulating the natural behavior of evaporites (e.g., Weijermars et al., 1993; Couzens-Schultz et al., 2003). The density of the polymer at room temperature is 972 kg/m^3, and the viscosity is 1.6×10^4 Pa·s when deformed at an experimental strain rate of 1.83×10^{-4} cm/s (Dell'Ertole and Schellart, 2013). Hereinafter, the term *model salt* will be used as substitute to the polymer and the standard salt tectonics terminology used when describing polymer-related structures. The scaling parameters are shown in Table 1.

2.3. Design, set up and experimental procedure

An experimental rig consisting of two glass-sided walls, a fixed wall, and a moving backstop wall with precontraction dimensions of 70 cm long, 50 cm wide and 30 cm high was used (Fig. 1a). A strong plastic sheet was set at the base of the deformation rig; the plastic sheet is undeformable under the modeling conditions and maintains its length during experiments. While walls remained static during the downbuilding stage, the mobile backstop wall was pushed forwards by a software-controlled servo motor at a fixed velocity of 4 mm/h.

Table 1
Dynamic scaling of the analog modeling experimental program. The scaling ratio is the Model to Nature ratio of a given magnitude or parameter.

Parameter	Equation	Model	Nature	Scaling ratio
Length		1 cm	1 km	10^{-5}
Density				
Sand/Brittle Rocks		1500 kg/m^3	2567 kg/m^3	0.58
Polymer/ Décollements		972 kg/m^3	2200 kg/m^3	0.4
Gravity		9.8 m/s^2	9,8 m/s^2	1
Cohesion		55 Pa	50×10^6 Pa	1.1×10^{-6}
Deviatoric stress	$\sigma = \rho \cdot g \cdot L$	121 Pa	2.34×10^7 Pa	5.2×10^{-6}
Ductile layer viscosity		1.6×10^4 Pa·s	10^{18} Pa·s	1.6×10^{-14}
Strain rate	$\varepsilon = \sigma/\eta$			3.24×10^8
Time	$t = 1/\varepsilon$	1 h	37,000 y	3.1×10^{-9}
Velocity	$V = L \cdot \varepsilon$	0.5 cm/h	13.5 mm/y	3.24×10^3

σ, deviatoric stress (Pa); ρ, density (kg/m^3); g, gravitational acceleration (m/s^2); L, length (m); ε, strain rate; η, viscosity (Pa·s); t, time (s); V, velocity (m/s).

The experimental setup consisted of a polygonal framework of minibasins with boundaries that were oriented at 60° and −60° with respect to the shortening direction (Fig. 1a). The model salt was laid on the basal plate from the backstop to a distal pinch-out located 55 cm away; laterally equivalent sand was added for the remaining 15 cm of the basal plate up to the opposite fixed vertical wall. The minibasins and salt ridges domain occupied a total stretch of 40 cm towards the hinterland. The experiments included three stages (Fig. 1b): an initial stage (Stage 1) where minibasins sank by downbuilding into model salt, and salt ridges grew vertically; sedimentation rate was adapted to keep up a balance between salt rise, minibasin sinking and sedimentation, to prevent burial of salt ridges or extensive salt extrusions. In consequence, the resulting sedimentation rate fitted an exponential trend; such balanced situation is found throughout Model 1 but varies laterally in Models 2, 3 and 4 (see Section 3.1.1). A second stage (Stage 2) where sedimentation rate outpaced the model salt rise rate. A third stage (Stage 3) of contractional deformation during which these structures were reactivated and squeezed and folding and thrusting occurred.

The initiation of salt evacuation by downbuilding (Stage 1) was triggered by pouring the first sand layer around the location of what would be the minibasin depocenters (Fig. 2). Downbuilding represents the syndepositional growth of a diapir whose exposed crest rises as sediments accumulate around it; the base of the diapir subsides together with the encasing strata, as the basin fills with sediment. Since poured loose sand creates a sedimentary lateral gradient (enhanced by a higher density than model salt; see Table 1), minibasins sank upon the onset of differential sedimentary loading (e.g. Rowan and Vendeville, 2006; Callot et al., 2016; Warsitzka et al., 2013; among others). Subsequently, new sand layers were sprinkled away from the minibasin depocenters, prograding towards the growing ridges (Fig. 1a). The experimental procedure was designed to generate outward expanding minibasins from a central seeding horizon reproducing bowl minibasins (Rowan and Weimer, 1998; Jackson et al., 2019; Fig. 2). Minibasins had a rhomboidal geometry whose long and short axes were 15 cm and 9 cm long, respectively (Fig. 1a). Stage 2 involved a higher sedimentation rate that tended to cover some of the growing salt ridges (Fig. 1b). The tested parameters included: 1) the thickness and geometry of the model salt, from constant to along-strike tapered; and 2) the syncontractional sedimentation rate (Table 2).

A total of 4 experiments were carried out: Model 1 involved a 12 mm thick horizontal model salt. Conversely, Models 2, 3 and 4 included a tapered model salt with a 2 to 22 mm thickening trend perpendicular to the subsequent shortening direction (Fig. 1). Note that in these three experiments the model salt thickness at the center of the model was like that of model Model 1 (12 mm thick). Lateral changes in the model salt thickness were achieved by tilting the deformation rig by 2.3°. The model salt was set to rest until its top was horizontal to avoid undesired flow. The rig remained tilted during the whole experiment and the upper surface was initially horizontal prior to shortening (Fig. 1).

Syncontractional sedimentation was absent (Models 1 and 2), low (Model 3) and high (Model 4) and was performed by increasing the regional level adding 2 mm thick layers each 12.5 mm or 5 mm of shortening in Models 3 and 4 respectively (Table 2). During shortening, allochthonous salt sheets were manually removed to minimize interactions with syncontractional layers. Total shortening was 5.5 cm for model Model 1, and 7.5 cm for Models 2, 3 and 4; these represent 8% and 11% of shortening, respectively.

2.4. Data capture and analytical techniques

To facilitate structural interpretations, the sandpack was built by alternating layers of colored sand. Colored circular polymer plugs were added within the model salt at the base of sinking minibasins and the base of salt wall intersections to track model salt flow during the experimental procedure (Dooley et al., 2009; Ferrer et al., 2017).

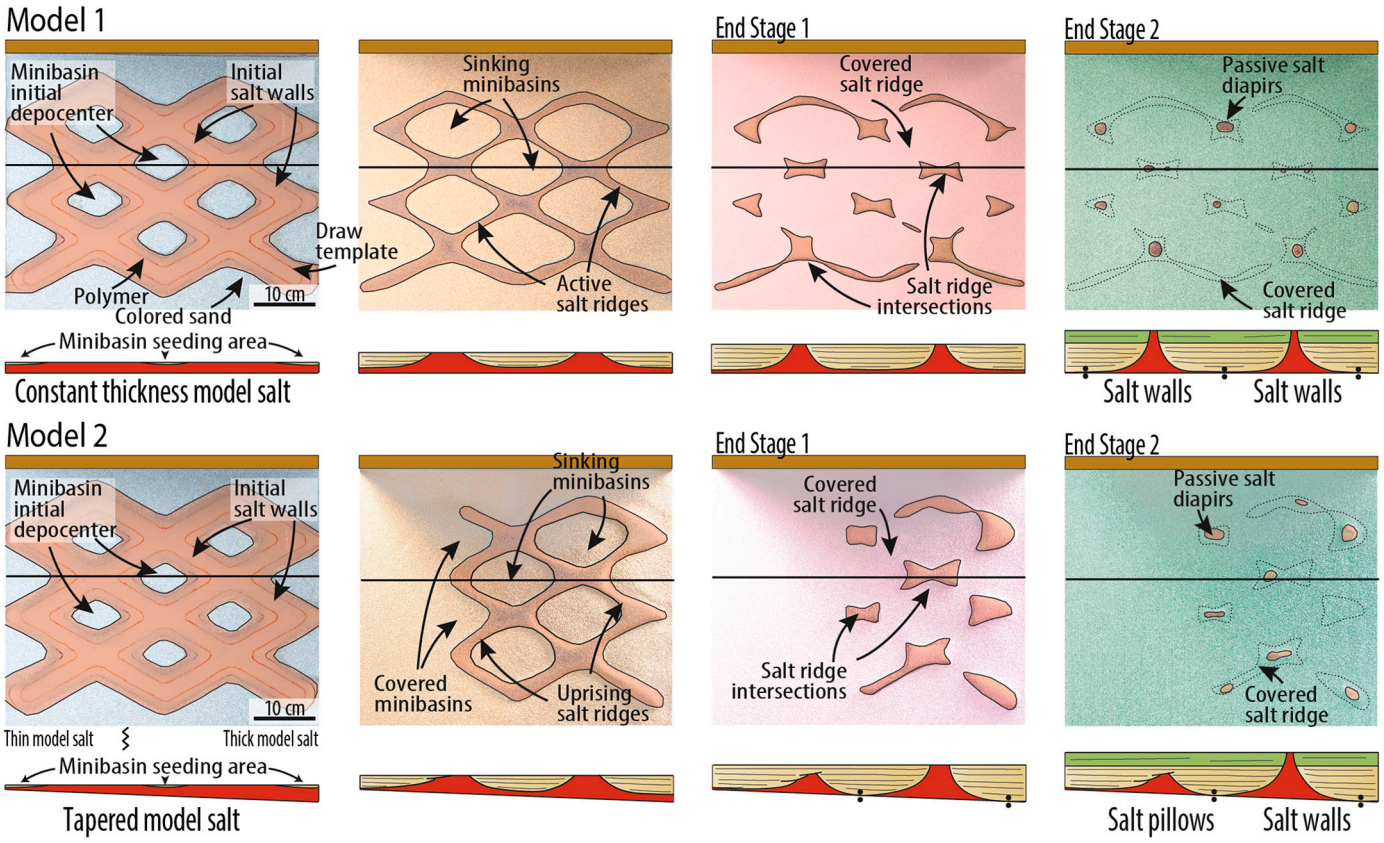

Fig. 2. Evolution during downbuilding (Stages 1 and 2) of the constant thickness model salt experiment (top, Model 1) and the tapered model salt experiments represented by Model 2 (bottom). The evolution is illustrated by top view pictures and interpretative sketches of inline sections (i.e. black lines on top views).

Table 2
Experimental program and tested parameters.

Experiment	Model salt thickness (mm)	Shortening (mm)	Syncontractional sedimentation rate (mm/mm of shortening)	Syncontractional sedimentation thickness(mm)
Model 1	12	55	0	0
Model 2	2–22 (Tapered)	75	0	0
Model 3	2–22 (Tapered)	75	0.16	12
Model 4	2–22 (Tapered)	75	0.4	30

Finally, for those models without syncontractional sedimentation (i.e. Models 1 and 2), an orthogonal grid was overprinted on the surface as a strain marker to record structural evolution.

Four techniques were used to analyze the experimental results: 1) Programmed computer-controlled time-lapse top-view and oblique-lateral high-resolution photographs to ensure the continuous monitoring of the morphometric evolution of models; 2) Particle Image Velocimetry (PIV) to characterize the kinematics of growing structures; 3) serial slicing of the experiments. These sections were interpreted and used as seeds to generate 3D image voxel reconstructions of the internal geometry of the models (Fig. 3); 4) step-by-step restoration of the interpretations of selected serial sections.

Section restorations have been used to reconstruct the stepwise evolution of selected sections (Roma et al., 2018). Analog modeling yields a huge control for restoration parameters that, in nature, are usually sources of uncertainty: i) the surficial structural traces can be tracked, ii) the displacement vector field quantified after sectioning and PIV techniques and iii) stratigraphic thicknesses are known. Restoration of sections further complements other observations regarding the geometrical and kinematical evolution.

3. Experimental results

3.1. Influence of the model salt geometry

3.1.1. Downbuilding stage

During downbuilding (Stage 1) minibasins sank while salt walls grew, and salt stocks formed at the intersection of salt walls. Downbuilding on a constant thickness model salt resulted in a symmetric pattern of salt walls, stocks and minibasins (Fig. 2, Model 1). Minibasins were primarily welded across the model at approximately the same time, reaching similar depositional thicknesses; in the same way, flanking salt walls attained the same elevation. From the end of Stage 1 until the end of Stage 2 all salt walls were covered by sand whereas growth of intervening stocks persisted with model salt flaring and extruding onto the model's surface (Fig. 2, Model 1).

On the other hand, for those models with a tapered model salt (Models 2, 3 and 4), downbuilding resulted in an asymmetric minibasin pattern (Fig. 2, Model 2). Given the constant applied syndownbuilding sedimentation rate for each time step, a thick model salt allowed persistent minibasin formation and model salt upwelling. On the contrary, for thin model salt under the same syndownbuilding sedimentation rate, incipient structures were buried earlier (during Stage 1), and thus minibasins and salt walls were hardly or not developed.

The graph in Fig. 1c shows the relation between minibasin thicknesses at the end of Stage 1 and original model salt thickness. The plot shows that for an original model salt thickness of 4–8 mm, downbuilding was only active during a relatively small period of time, whereas for

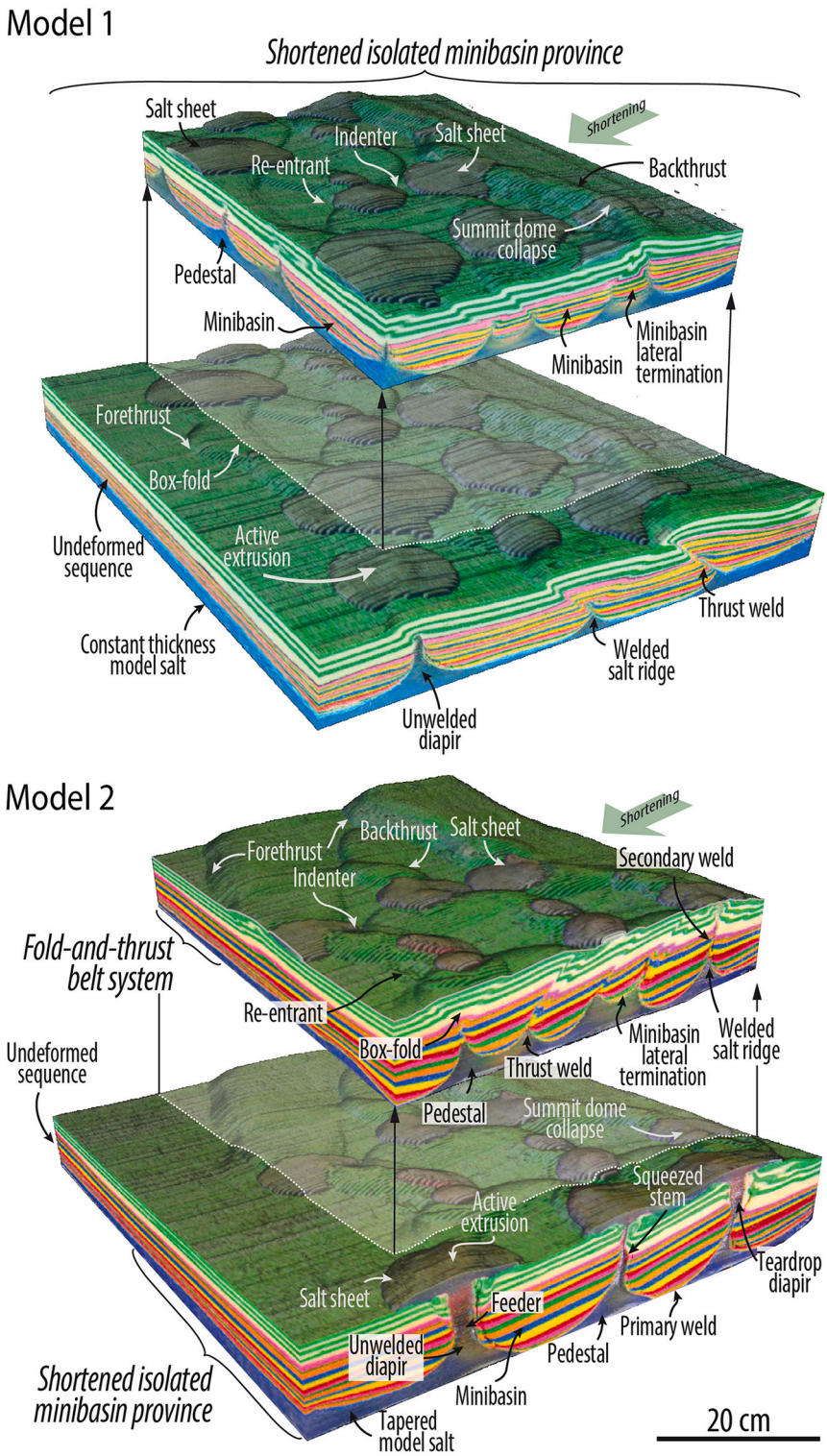

Fig. 3. 3D voxels showing the characteristic structural styles of salt-related and fault-related structures of the constant thickness model salt experiment (Top, Model 1) and along-strike tapered model salt experiments, illustrated by Model 2 (bottom). Dark green areas correspond to model salt surficial extrusions. Top panels represent a cropped volume from the overall model. (For interpretation of the references to colour in this figure legend, the reader is referred to the web version of this article.)

model salt thicknesses lesser than ca. 4 mm, downbuilding was never an active process. Then, over a threshold value ranging between 8 and 12 mm of original model salt thickness, minibasins' thickness increased linearly with that of the original model salt.

To summarize, our modeling shows that the role of the original model salt thickness in downbuilding processes is paramount, with formation of isolated minibasin provinces where model salt was originally thick and an undeveloped domain of horizontally layered sand over a static thin model salt. The transition between these domains consists of a system of salt pillows (Figs. 1c and 2).

3.1.2. Surface evolution during contraction

Common structural features were found through all the experiments: closing of salt ridges led to roof arching or box-folding, and backthrusts formed parallel to salt ridges, converging into the salt diapirs- and resulting into a polygonal pattern that mimics the inherited structural grain. The occurrence of indenters and reentrants (Dooley et al., 2009; Santolaria et al., 2021) (Figs. 3, 4a) points out that squeezing of salt stocks took place by forward displacement and indentation of the more rigid minibasins into these salt diapirs. Model salt squeezing led to formation of salt sheets (Fig. 3). In those models featuring tapered model salt, the inherited asymmetry structural architecture had a profound control on the structural styles developed by shortening. Contractional salt-related deformation dominated the isolated minibasin province, whereas a salt-detached fold-and-thrust belt formed from the thin model salt domain (Figs. 3 and 4). The impact of the model salt thickness distribution was not limited to the structural styles but also to the kinematics of the distinct structural domains (Figs. 3–5).

At the onset of contraction, shortening rapidly rejuvenated salt stocks as evidenced by salt extrusions. Further shortening resulted in the reactivation of the innermost salt ridges as well (Fig. 4a, 5a, 12mm of shortening). In Model 1, salt stock's rejuvenation and salt ridge's reactivation occurred symmetrically and reflected the inherited down-building pattern (Fig. 4a, 12mm of shortening). Conversely, in Model 2, reactivation of the innermost salt ridges graded into a foreland-directed frontal thrust striking nearly perpendicular to the shortening direction across the thin model salt domain (Fig. 5a, 12mm of shortening). In Model 1, additional shortening led to formation of a frontal thrust running parallel to the outermost salt ridge (Fig. 4a, 36 mm of shortening). In Model 2, across the isolated minibasin province (i.e. the thick model salt domain), reactivation of ridges occurred progressively from the hinterland to the foreland (from 12 mm to 60 mm of shortening; see Fig. 5a). Along strike, deformation graded from an area where squeezed salt stocks are linked by thrusts mimicking the inherited pattern of salt ridges to a set of linear thrusts; this change coincides with the transition from a well- to a hardly developed salt-sediment system. (Fig. 1c).

3.1.3. Section view and structural style evolution during shortening

As revealed and illustrated by the restoration of four sliced sections from Model 2 (Fig. 6), structural styles and related kinematics have been grouped into four different types: two of them are exclusive to the

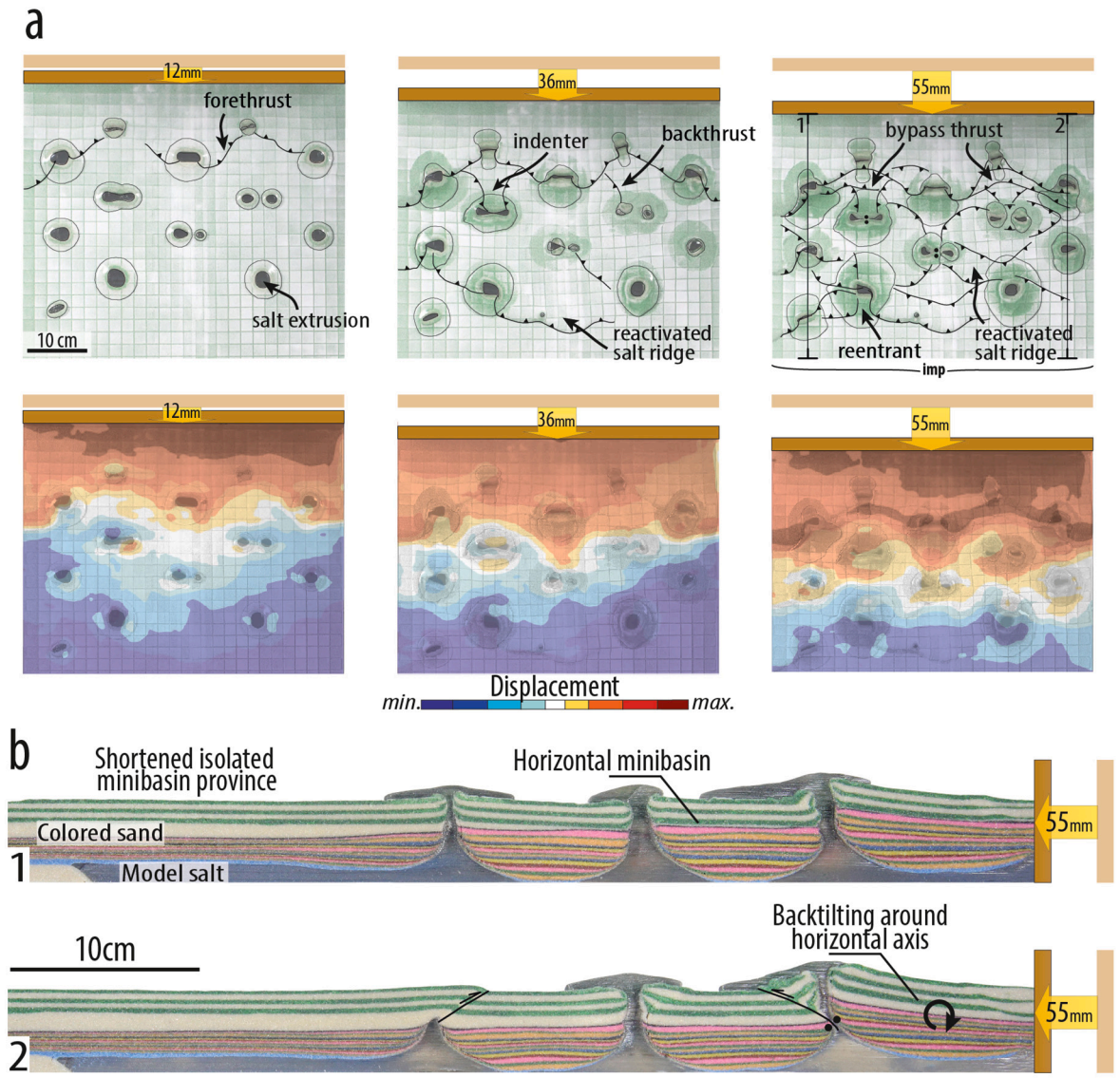

Fig. 4. a) Evolution during shortening of the constant thickness model salt experiment (Model 1) illustrated by a) interpreted top view pictures (top) and displacement vector fields (bottom). imp: isolated minibasin province. b) Sections at the end of shortening highlighting the symmetry of this experiment (See location in a).

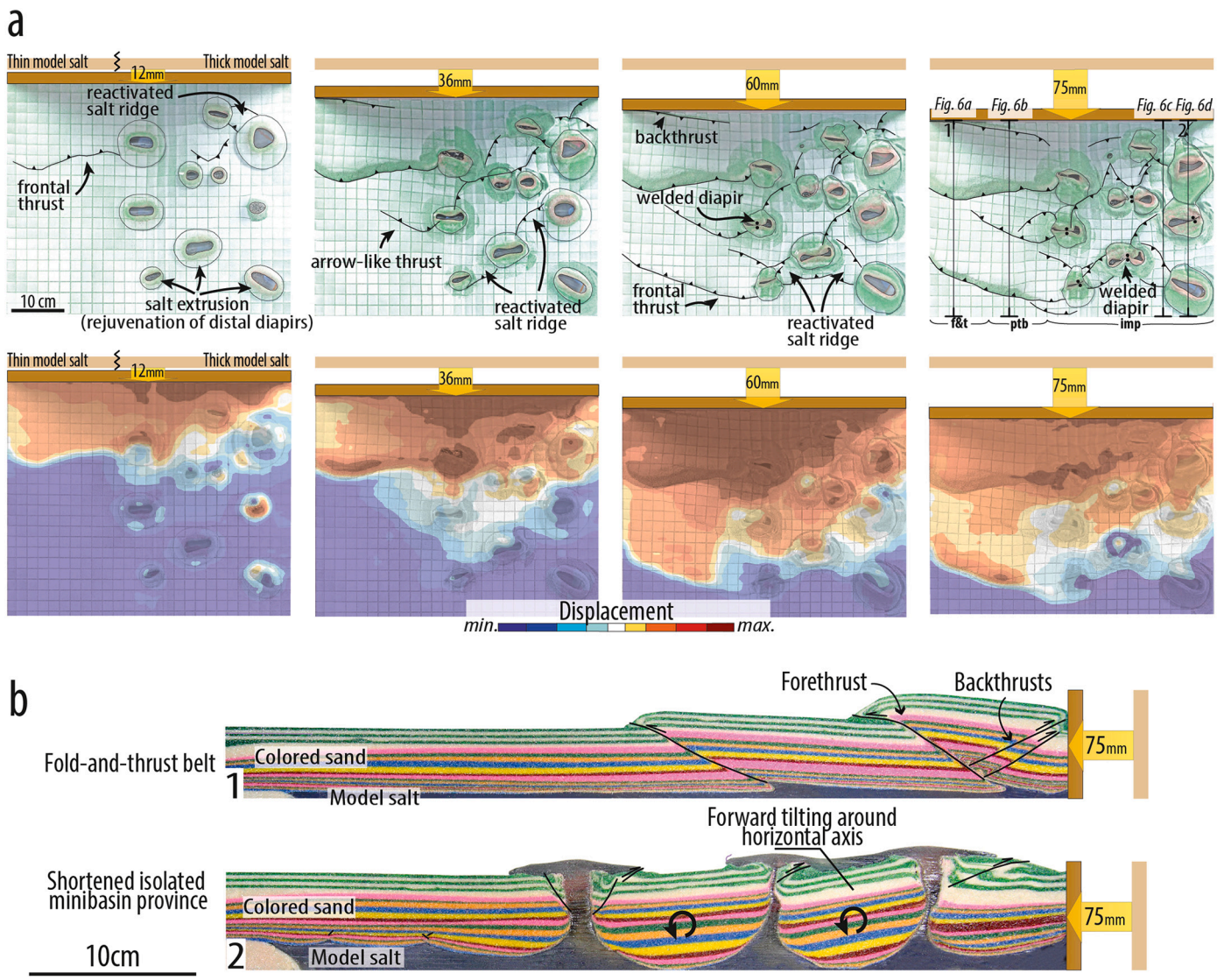

Fig. 5. a) Evolution during shortening of tapered model salt experiments represented by Model 2 and illustrated by a) interpreted top view pictures (top) and displacement vector fields (bottom). f&t: fold-and-thrust belt; ptb: pillow thrust belt; imp: isolated minibasin province. b) Lateral sections at the end of shortening highlighting the asymmetry of this experiment. Note the location (see a) of the sections is equivalent to the sections in Fig. 4.

tapered model salt experiments and the other two are common to all the experiments. The first two types comprise the contraction of i) a constant thickness, horizontal model salt-sand sequence, where shortening led to the growth of a regular salt-detached fold-and-thrust belt with asymmetric thrust-related folds detached on thin model salt (Fig. 6a); and ii) a salt-pillow thrust belt formed from a poorly developed salt system (Fig. 6b). The other two include the contraction of well-developed salt-minibasin systems and resulting from the deformation of iii) salt ridges and minibasin edges (Fig. 6c) and iv) salt stocks and minibasin depocenters (Fig. 6d). All these structural styles correspond to a geometrically distinct but kinematically compatible contractional evolution. In broad terms, and regardless of the structural style, deformation propagated forwards while hinterland structures remained active (i.e. synchronous thrusting).

Considering the thin model salt domain (<4 mm) of Model 2, contractional deformation represents a regular, salt-detached, fold-and-thrust belt (Fig. 6a). The forward-developing thrust wedge grew sequentially and displays a taper angle of 5 degrees. Importantly, there is no correlation between thrust spacing or their nucleation points, and the along strike salt wall and minibasin design pattern (Fig. 1).

Along strike into thicker model salt (Fig. 6b), the preshortening configuration features a series of salt pillows distributed according to the original geometrical design (Fig. 6b). Salt pillows represent weak discontinuities that controlled the nucleation of thrusts and number of structures developed during shortening; in this case, three thrusts form rather than two as in the previous situation (Fig. 6b). The salt-pillow thrust belt is characterized by a dominant forward vergence of thrusts which emplaced following a forward-breaking sequence.

Within the isolated-minibasin province, we first focus on the evolution of the salt ridges and minibasins' lateral edges (Fig. 6c). At the beginning of the contractional stage, proximal salt ridges (i.e those close to the moving backstop wall) were preferentially squeezed, as evidenced by arched roofs, and acted as nucleation zones for thrusting and backthrusting (Fig. 6c). This deformation predated the transference of deformation to the distal salt ridges which remained, at this time, undeformed. Ongoing shortening resulted in further reverse faulting, foreland propagation of deformation and additional squeezing of salt ridges. Salt ridges became eventually closed along vertical secondary welds that became nucleation points for shorter-wavelength thrusts (Fig. 6c). Salt ridges closure and welding occurred in a *zip-like* mode as welded ridges nucleated faulting at progressively lower structural levels and involving deeper parts of the minibasins (Fig. 6c). Across the salt

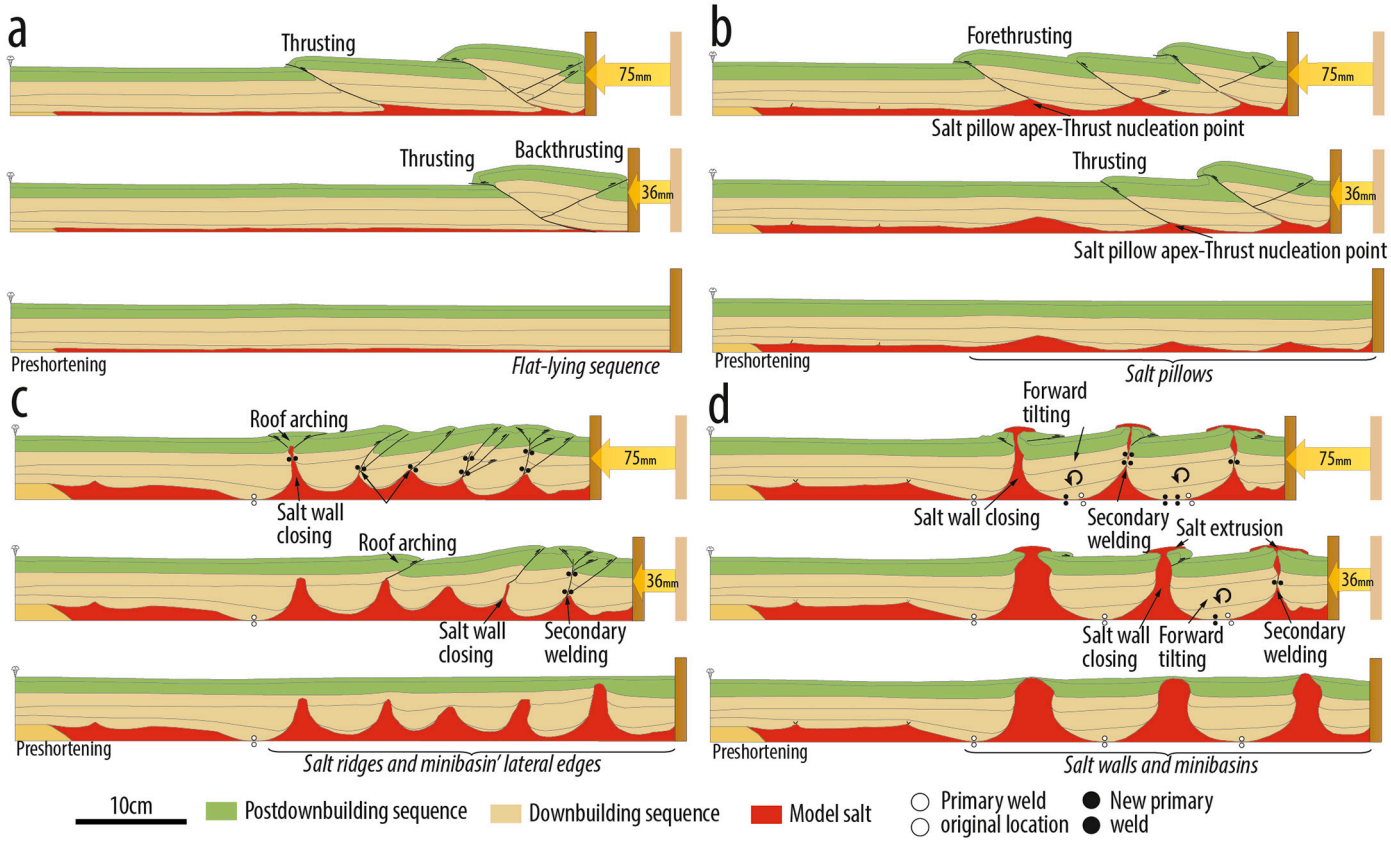

Fig. 6. Sequential restoration of four representative cross-sections from Model 2. The sections illustrate kinematic evolution of a) the fold-and thrust belt system, b) the salt pillow thrust belt and transects through c) salt ridges and minibasins' lateral edges and d) salt walls and minibasins. See location in Fig. 5a.

walls and minibasins transects (Fig. 6d), mild shortening is accommodated by narrowing of salt stocks whereas minibasins are mostly transported forwards attaining less deformation. As salt stocks closure continued, the proximal minibasins underwent forward translation and, in some cases, tilting; distal minibasins however, remained in situ or were slightly transported forwards (Fig. 6d).

Tilting occurred both forward and backward. It is worth noticing that tilting of minibasins in Model 1 (i.e. constant thickness model salt) was rare and restricted to the minibasins attached to the moving backstop (Figs. 4b). Additional shortening entailed further stock closure and continuous extrusion of allochthonous salt. At the end of experiments, some of the diapirs remained opened whereas others were secondary welded (see secondary welds in Fig. 6d). Teardrop diapirs and pedestal remnants are found in association with secondary welded salt stocks (Fig. 3). Thrusting is uncommon and when it occurs, it is associated with welded salt bodies whose secondary welds act as thrust nucleation points (Fig. 6c).

3.2. *Influence of syncontractional sedimentation rate*

3.2.1. *General geometries and kinematics*

In this section, we consider those experiments featuring a tapered model salt (Models 2, 3 and 4). At the onset of shortening, salt stocks were squeezed leading to salt extrusions. With ongoing shortening (Figs. 7, 12 mm of shortening), a frontal thrust occurs along the thin-model salt domain while salt walls located near the moving backstop were reactivated in the thick model salt domain (Figs. 6 and 7). In consequence, diapir roofs became arched, onlapped and eventually overlapped by syncontractional sediments (Fig. 8a). Later on, in the isolated minibasin province of Models 2 and 3, deformation affected most of the salt ridges. However, in Model 4 (highest sedimentation rate) deformation remained concentrated on the inner structures (Fig. 7c; after 36 mm of shortening).

Box-folds formed above the shortened salt ridges bounded by a backthrust and a younger thrust as observed at surface (Fig. 7) and recorded by syncontractional sand layers (Fig. 8b). In the salt-pillow thrust belt of Model 2 (i.e. no syncontractional sedimentation), deformation progressed forward with the occurrence of an *arrow-like* thrust, likely controlled by the inherited salt pillows (Fig. 7a, 36 mm of shortening). Conversely, deformation amplified the previously developed thrust in Models 3 and 4 (Fig. 7b, c, 36 mm of shortening), since syncontractional sedimentation hindered the forward propagation of deformation in both the salt-pillow thrust belt and fold-and-thrust belt domains.

In Model 2, further shortening (Fig. 7a, 60 mm of shortening) caused the development of a new frontal thrust encompassing the salt-pillow thrust belt and the fold-and-thrust belt domains, while the older thrusts propagated laterally from the center of the model (Fig. 7a). In Models 3 and 4, new thrusts also occurred, which are restricted to the salt-pillow thrust belt (Fig. 7b and c). Thrusting occurred in the form of a backthrust (Model 3, Fig. 7b) or a thrust (Model 4, Fig. 7c), both depicting curved surficial traces. Out of the isolated minibasin province, syncontractional sedimentation favored the amplification of previously developed hinterland structures resulting in thrusts with larger displacements and involving thicker successions (Fig. 9, sections a1, b1 and c1). At the end of the experiments after 75 mm of shortening, (Fig. 7), Model 2 showed more distributed deformation, with a denser framework of structures (i.e. more compartmentalization). In Model 4 (highest syncontractional sedimentation rate (Fig. 7c), deformation concentrated in a lesser number of structures, some of which were systematically shutdown by sediment burial (Fig. 9). In broad terms, syncontractional sedimentation delayed the propagation of deformation being enhanced with the increase in sedimentation rate.

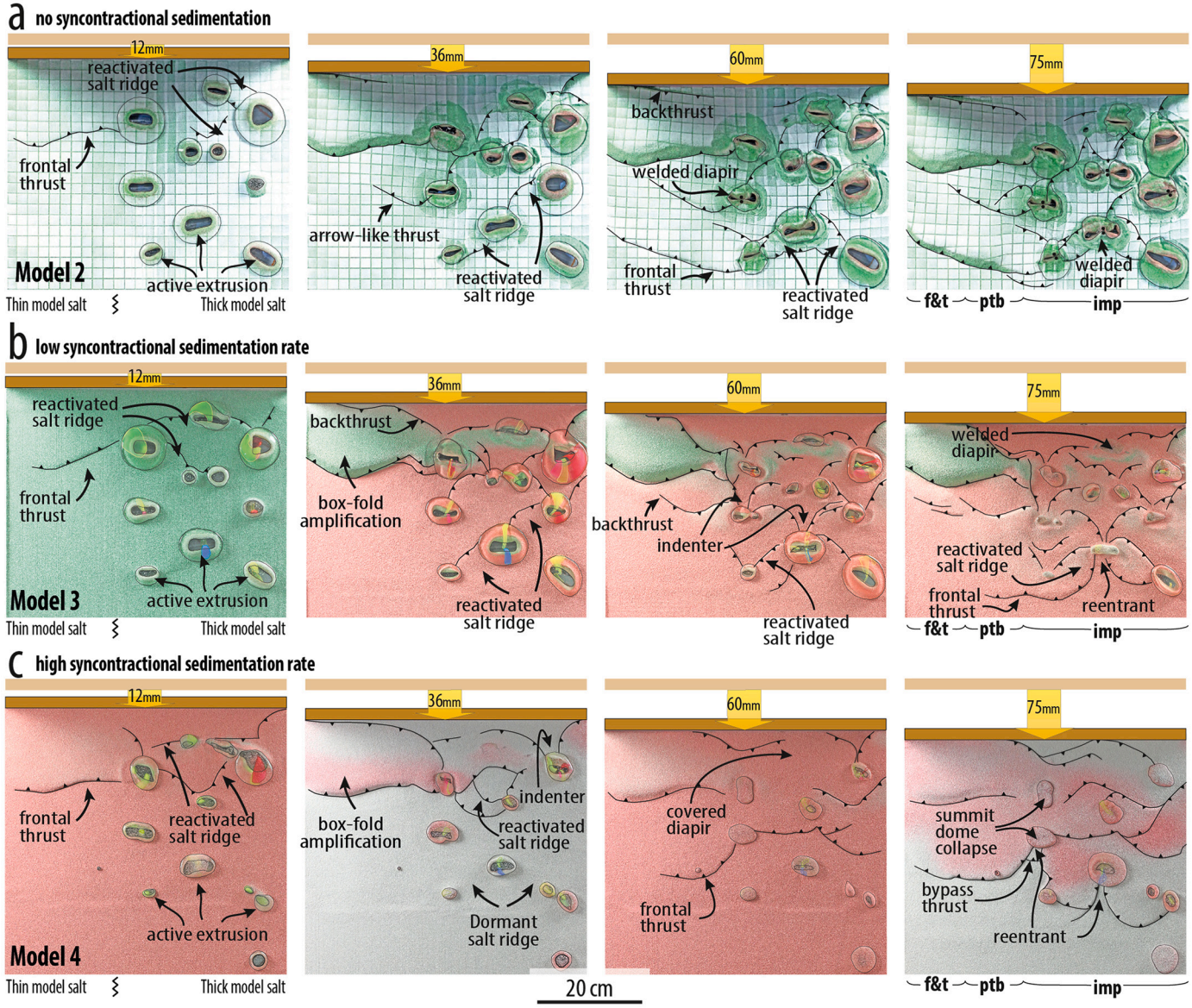

Fig. 7. Top view evolution of the experiments with a tapered model salt: a) Model 2, no syncontractional sedimentation, b) Model 3, low syncontractional sedimentation rate and c) Model 4, high syncontractional sedimentation rate at 12, 36, 60 and 75 mm of shortening. The labels f&t (fold-and-thrust belt), ptb (salt pillow thrust belt) and imp (shortened isolated minibasin province) refer to the structural styles and kinematic models summarized in Fig. 6 and explained in detail in Section 3.1.3.

3.2.2. *Syncontractional minibasin tilting*

Now we focus on the evolution on minibasins in the isolated minibasin province. During shortening, most of the minibasins underwent forward tilting by rotation around a horizontal axis normal to shortening direction (Fig. 9). Some exceptions, where tilting has a backward sense, are the minibasins attached to the moving backstop and a few cases in Model 4 that are discussed below.

Forward tilting led to the formation of growth sequences and onlap relationships in the syncontractional sand layers (Fig. 8c). Tilting angle increased with syncontractional sedimentation: from 6 to 7 to 12–17 degrees in sections a4 and b4 of Fig. 9, respectively. However, when the sedimentation rate exceeds a threshold (discussed later), in our case a value between 0.8 and 2 mm/h (sedimentation rates in Models 3 and 4), total tilting diminishes or even experiences counter rotation: from 12 to 17 degrees to 2–6 degrees in sections b4 and c4 in Fig. 9, respectively. Backtilting of minibasins during shortening is evidenced by hinterland-fanning growth strata whose sedimentary architecture registers a shift from a hinterland-directed onlap to a foreland directed onlap (Fig. 8d).

3.2.3. *Primary weld kinematics during contraction*

Prior to the shortening stage, minibasins have been primary welded. Primary welds are localized underneath the minibasins depocenter (Fig. 10). With shortening, these primary welds deform in a variety of ways that are tracked by sand remnants or polymer colour marker trails (Figs. 11 and 12). During contraction, some primary welds are sheared off by the forward displacement of the primary welded minibasins: these are herein named *sheared primary welds* (Dooley et al., 2019; Duffy et al., 2021): these welds remain fixed with respect the minibasin but have been laterally displaced (Fig. 11a.)

As minibasins undergo different degrees of tilting, primary welds either migrate in the sense of tilting or lengthen by rolling along the base of the minibasin defining *rolled primary welds* (Fig. 11b and c). In the first case, the original primary welds unweld at the same time new ones form (Fig. 11b). Alternatively, rolling and associated minibasin deformation can cause the original primary welded area to expand (Fig. 11c). Moreover, in Model 4, some of these sheared primary welds are also unwelded while minibasin are no longer in contact with the basement,

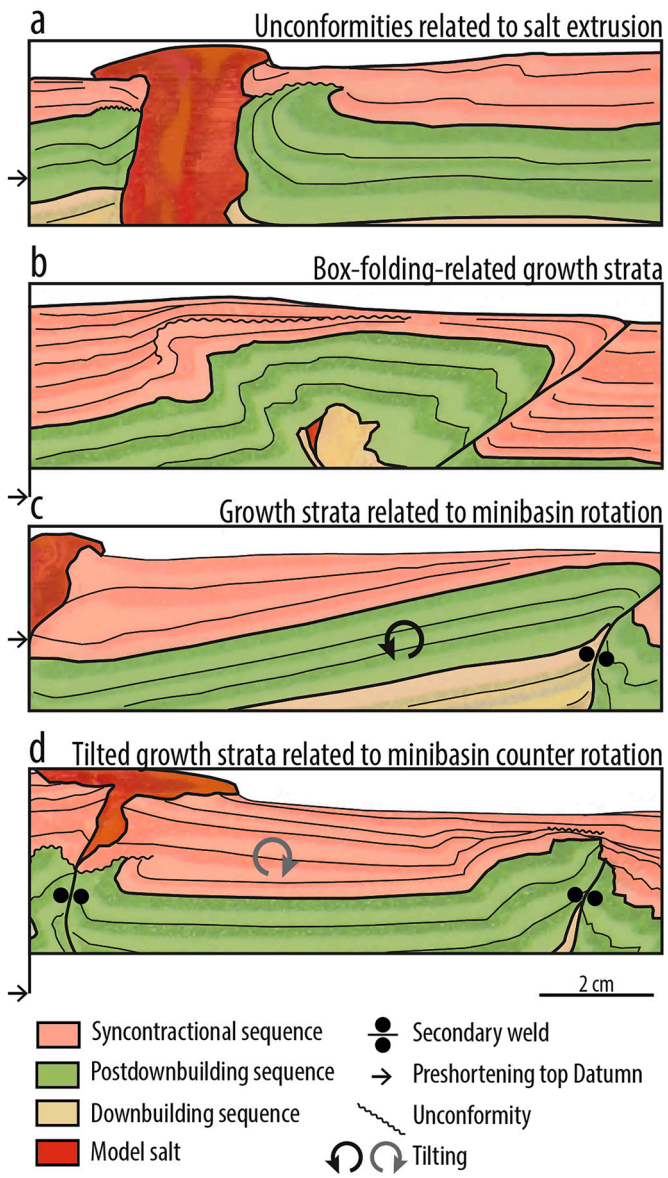

Fig. 8. Interpreted details of four examples of syncontractional sequence geometries that illustrate: a) the unconformities related to roof arching and salt extrusion (Model 3), b) growth geometries, condensed sequences and missing units associated with box-folding (Model 4), c) growth geometries that records tilting of minibasins (Model 3) and d) counter tilting (Model). See black frames in the cross sections of Fig. 9 for location.

defining *delaminated primary welds* (Fig. 8, sections c4, Fig. 11d and Fig. 13). Sheared primary welds are found in unrotated minibasins and thus are common in Model 2 where no syncontractional sedimentation was considered (Fig. 9). *Rolled primary welds* are related to tilting and therefore are observed in all the models having a tapered model salt, especially in Model 3, with moderate syncontractional sedimentation rate. Conversely, delaminated primary welds are exclusive of Model 4.

4. Discussion

Isolated minibasin provinces refer to areas where minibasins formed by downbuilding are completely surrounded by salt walls and stocks forming a polygonal array of isolated basins (Harrison and Jackson, 2014; Kergaravat et al., 2016; Duffy et al., 2018; Jackson and Hudec, 2017; Dooley et al., 2019; Strauss et al., 2020). Many of these salt provinces have been subsequently shortened either by gravitational failure of passive margins (Rowan et al., 2004; Jackson et al., 2008; Granado et al., 2016), or by convergence related to plate tectonics (Jackson and Harrison, 2006; Rowan and Vendeville, 2006; Granado et al., 2019). Some of these shortened isolated-minibasin provinces are outstandingly exposed, depicting steeply-dipping to overturned beds (e.g. Sivas basin of Turkey, Legeay et al., 2019) or, conversely, remain nearly horizontal (Central High Atlas, Calvín et al., 2018; Fars area, Zagros fold belt, Jahani et al., 2007). During contraction and due to the weakness of salt rock (Weijermars et al., 1993), contractional strain is focused on the salt body network whereas country rocks remain largely undeformed (Rowan and Vendeville, 2006). As a consequence, minibasins broadly preserve their original geometry, but can undergo translation, jostling, collision (Duffy et al., 2017) and rotations (Rowan and Vendeville, 2006; Ferrer, 2012; Callot et al., 2016; Duffy et al., 2021). Meanwhile, intervening salt bodies are squeezed which lead to the pressurization of salt, upwelling, flaring and eventual extrusion as allochthonous salt sheets (Nilsen et al., 1995).

In the following sections, we discuss how minibasins evolve in time during downbuilding and shortening, how deformation is transferred from the hinterland to the foreland and finally modeling results are compared to the Fars Salient and the Northern Calcareous Alps.

4.1. Minibasin growth, syncontractional tilting and primary weld evolution

In our experiments, which considered no external boundary conditions, incipient minibasins start as nearly symmetrical depocenters where subsidence is concentrated; continuous minibasin sinking is accommodated by model salt expulsion from beneath the minibasins (as in Dooley et al., 2019 and Duffy et al., 2021), resulting in broadly synformal-shaped depocenters, or bowl minibasins, hosted into mobilized salt (Trusheim, 1960; Rowan and Weimer, 1998; Vendeville, 2002). Basin-centered subsidence may continue as far as the source layer of salt is thick enough to account for minibasin sinking (Jackson and Hudec, 2017). In our modeling, minibasin growth can be represented by an exponential curve that clearly illustrates the relationship between time and minibasin thickness (Fig. 2b). Sedimentation of new layers is subordinate to the accommodation space created by minibasin sinking and hence sedimentary rate accelerates with time. Model sand density is much higher than that of model salt which controls this behavior. In fact, this assumes that sedimentation is continuous and overcomes topography creation. In nature, such rapid filling of the accommodation space is found in highly productive carbonate systems rather than clastic systems (e.g. Strauss et al., 2020).

Later, salt flow from beneath the minibasin slows down as welding approaches or is completed and so, boundary drag forces dramatically oppose additional flow (Waltham, 1997; Wagner III and Jackson, 2011). It is worth noting how critical the model salt geometry is regarding the formation of minibasins and surrounding salt structures. Our experimental approach was designed to permit primary welding but to avoid sinking of the flanks and formation of turtle structures. As a result, concave minibasins with steeply-dipping flanks, salt bodies featuring well-developed pedestals and localized primary welds formed. In other words, minibasins are nearly symmetric across strike (i.e., *bowls*), hence, the system can be considered as initially balanced. Yet, it is potentially unstable since minibasins laid on a reduced pivoting point (i.e. the primary weld) and are free to move as they are surrounded by salt. Instability is counteracted by regional sedimentation that binds minibasins together and make them less independent.

In contrast to other analog modeling works dealing with the contractional reactivation of isolated minibasin provinces (Rowan and Vendeville, 2006; Ferrer, 2012; Duffy et al., 2021), the experiments presented here showed no evidence for minibasin rotations around vertical axes. One of the most plausible reasons has to do with the sizes and shapes of the minibasins as already outlined in the seminal work of Rowan and Vendeville (2006). If minibasins present different sizes,

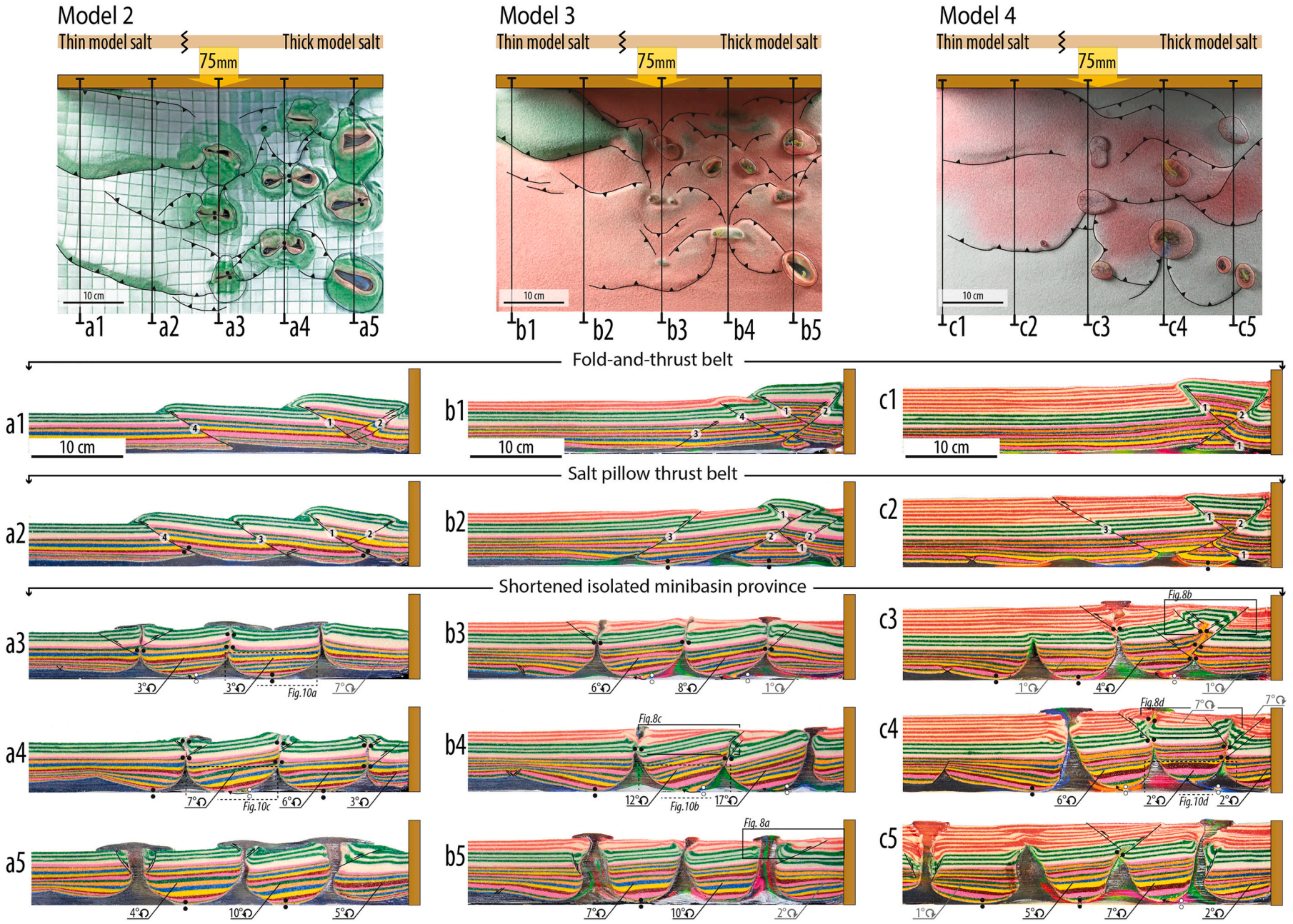

Fig. 9. Top views (top) and representative cross-sections (bottom) of Models 2, 3 and 4 at the end of shortening.

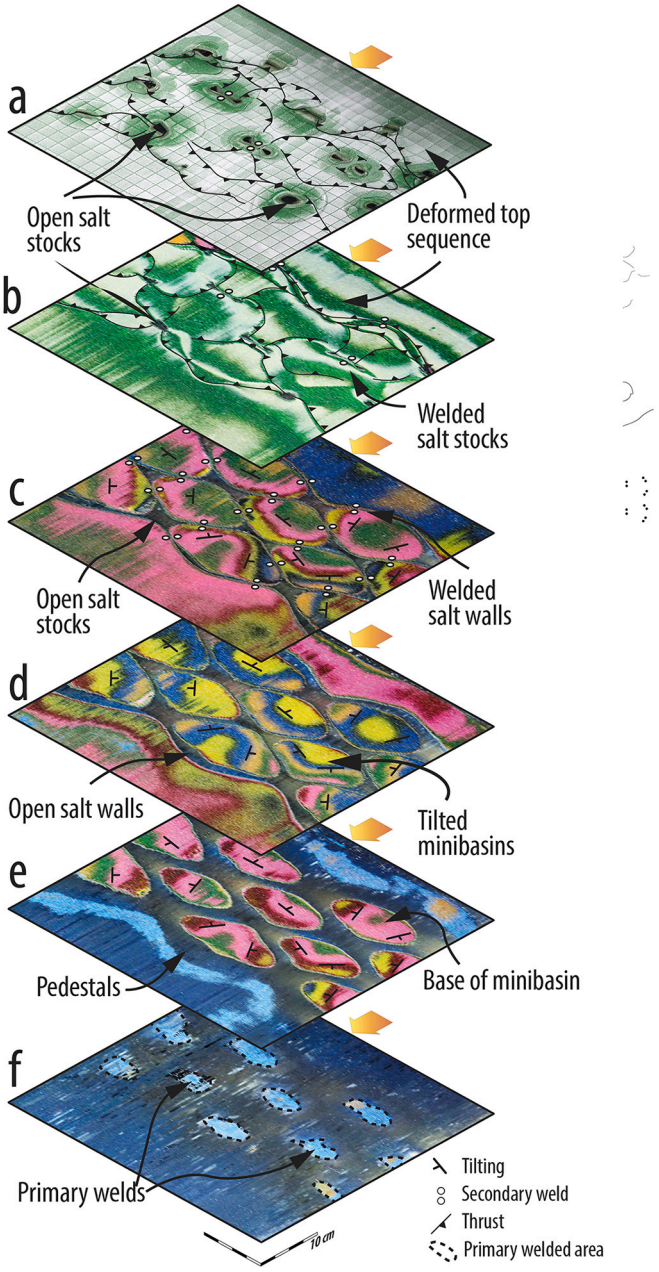

Fig. 10. Interpreted depth slices of Model 1. Depth slices are extracted from a 3D voxel of the model built from serial cross sections (spacing 3 mm) at the end of the experiment. a) top view of the model surface showing the polygonal pattern of the contractional structures and how some salt stock remained opened after contraction. b) shows the deformation characteristic of the topmost sand sequence. c) net of secondary welded salt walls showing how minibasin get into contact by their sides rather than the axis. d and e) tilted minibasin and pedestals. f) depth slice at the base of the models showing the areal extension of primary welds.

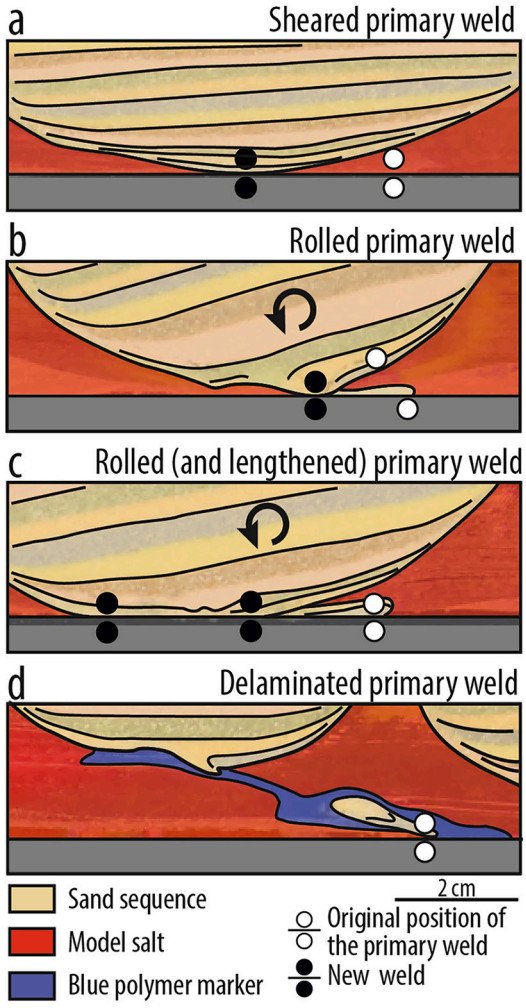

Fig. 11. Interpreted details of a) sheared, b) rolled, c) rolled and lengthened and d) delaminated primary welds. See dashed black frames in the cross sections of Fig. 9 for location.

shapes and aspect ratios, squeezing of intervening salt can allow for vertical axis rotations, and jostling between minibasins. On the other hand, in our experiments minibasins only experienced horizontal axis rotation due to i) the presence of a thick and, thus, strong roof and ii) a regular pattern of minibasin architecture that also prevent for vertical axis rotation. Given the amount of shortening in our experiments, an obvious corollary is that to undergo vertical axis rotation, minibasins need unconstrained boundaries and contrasting aspect ratios as well as differing orientation with respect to the shortening direction.

During contraction and detached along the basal model salt which acts as a *décollement* previously developed minibasins may undergo forward displacement and tilting. These processes depend on several factors: i) the amount of shortening (e.g., Ferrer, 2012); ii) the syncontractional sedimentation rate (Fig. 9); iii) the original shape of minibasins (e.g., Rowan and Vendeville, 2006), iv) the orientation of the salt ridge network with respect to the shortening direction (e.g., Rowan and Vendeville, 2006; Ferrer, 2012); and v) the amount of remaining salt and enveloping salt flow patterns (e.g., Callot et al., 2016; Duffy et al., 2021).

Nearly vertical minibasins flanks favors indentation and the formation of vertical secondary welds. Conversely, more gentle flanks may promote imbrication (Callot et al., 2016). Shortening leads to the forwards displacement of minibasins and their primary welds and pedestals in between; if the bounding salt walls are secondarily welded the juxtaposed minibasins are also transported forwards (Fig. 13). This overall displacement led to the modification of the architecture of the system, including the original location of primary welds whose forward displacement along the base resulted in sheared primary welds (Figs. 11 and 14).

In our experiments, tilting of minibasins has a dominant forward sense. This is most likely triggered by the abounding backward vergence of thrusting (i.e. backthrusts). Even though the limited offset of these backthrusts at the beginning of shortening, it is enough to promote forward tilting of the minibasin. Forward tilting is lately enhanced by the resistance exerted by primary welds acting as pivot points and new syncontractional sand layers. Rolled primary welds (Fig. 14) evolution is

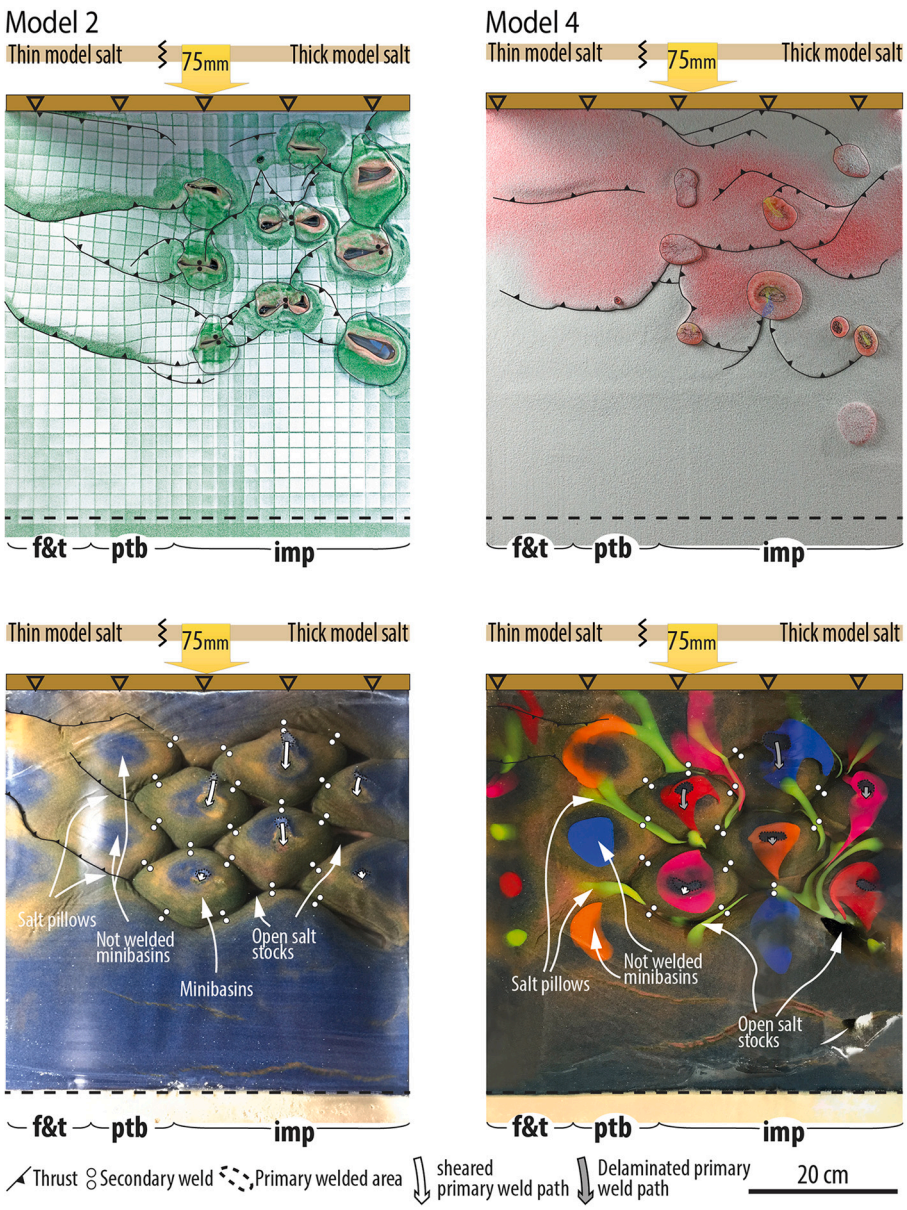

Fig. 12. Top view of the surface (top) and the bottom view of the base (bottom) of Model 2 (left) and Model 4 (right). Top views show the main surficial traces of folds and thrusts and the open and extruding diapirs. Bottom views display the basal transparent polymer (and colored marker plugs in the Model 4) which allows visualize the shape of minibasins, the branch line of thrusts, the location of secondary welds and primary welds and track their paths during shortening. f&t (fold-and-thrust belt), ptb (salt pillow thrust belt) and imp (shortened isolated minibasin province) labels refers to the structural styles and kinematic models summarized in Fig. 6 and explained in detail in Section 3.3. Black empty triangles represent the location of cross-sections in Fig. 9.

characterized by a continuous migration of the primary weld together with a significant amount of tilting of minibasins (up to 12°). The architecture of syncontractional sequences responds to the forward leaning minibasins as shown by growth strata geometries (Figs. 7 and 8). Growth strata geometries record the continuous tilt through the experiments, as well as the forward displacement of minibasins leading to a combination of sheared and rolled primary welds (Fig. 14).

A relevant observation in our experiments is that minibasin tilting is enhanced in the model that involves a low sedimentation rate (Model 3) whereas higher sedimentation rates (Model 4) hamper it (Fig. 13, 55 mm of shortening). This suggests the existence of a specific syncontractional sedimentation rate threshold over which minibasin tilting slows down or even swifts from forwards to backwards. The influence of syncontractional sedimentation may be interpreted as the result of the delay of shortening propagation to the foreland, which leaves less time and thus less shortening to affect the distal minibasins, effectively more largely buried under sediments. Alternatively, it may be interpreted by the direct effect of differential loading caused over specific minibasins by uneven sedimentation. Once tilted, the addition of new syncontractional layers always increases the differential stratigraphic load over minibasins and in consequence it favors the ongoing tilting trend. Quantitatively speaking, however, higher syncontractional sedimentation rates produce a broader distribution of the sedimentary load and therefore less differential loading, increasing the roof strength and making the minibasins interdependent. In this situation, it may be easier (in comparison to lower syncontractional sedimentary rate scenarios) for other external factors to counteract the forward tilting trend. For example, secondary welding of salt diapirs and salt walls can cause minibasin rotation to stop. After secondary welding, minibasins can become locked-up and act as a mechanically strong beam. A stronger beam of connected minibasins can accommodate additional shortening through forward displacement and inflation of salt at the base (Fig. 11d and 13, 75 mm shortening). In this scenario, primary welds become unwelded and minibasins delaminated. Shifts on tilting sense are reflected by changes in the geometrical pattern of syncontractional sedimentation: growth strata shifts and opposes previous trends (Figs. 8 and 13, 55 to 75 mm of shortening). This reflects the last stage in the evolution of sheared and rolled primary welds with the delamination of primary welds (Figs. 11, 13 and 14).

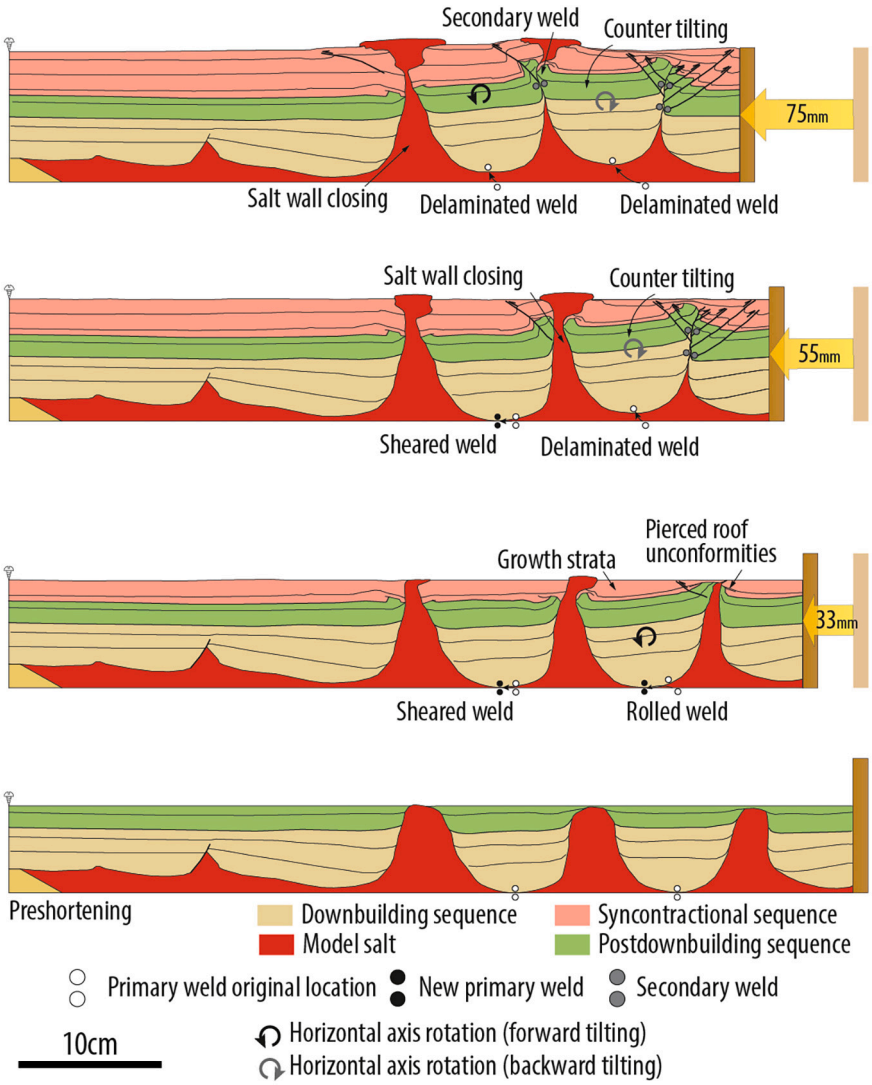

Fig. 13. Stepwise restoration of a representative cross-section of Model 4 (section c4 in Fig. 9) where main deformation events are labelled. See Fig. S1 in supporting information for a complete restoration from downbuilding to the end of the experiment.

4.2. Shortening distribution and deformation transfer

Our experimental models highlight how an along-strike tapered basal salt controls the preshortening evolution of the salt system and the resulting geometries led to contrasting structural styles and kinematics during contraction. In this sense, two clear end-members can be differentiated: i) if salt is thin enough, a fold-and-thrust belt characterized by synchronous thrust activity within a dominant breaking-forward thrust sequence; in this case, thrust spacing was controlled by the thickness of the brittle-ductile sequences and, to some extent, by coupling with the adjacent salt pillow system; and ii) a shortened isolated minibasin province characterized by necked-off salt bodies, forward translation and tilting of minibasins. In between both, the influence of the inherited pattern is still appreciable in a situation where salt pillows localize contractional deformation regardless their orientation with respect to the shortening direction (Jackson et al., 2011; Callot et al., 2012; Ferrer, 2012; Dooley et al., 2013; Moretti et al., 2013). The key observation is that no matter the structural geometries the whole wedge system maintains along-strike kinematic compatibility. Thus, one of the most relevant results of our modeling is that while the amount of shortening is the same for a given salt-influenced fold-and-thrust belt it can result in contrasting structural styles. The total shortening accommodated by slip along thrusts must be equal to that generated by squeezing and necking of weak salt which tends to be cryptic. Section restoration of salt-related contractional systems is always challenging (Granado et al., 2019; Rowan and Ratliff, 2012). As derived from our results, structural restoration of serial cross-sections in fold-and-thrust belts is a complementary constraint when assessing shortening estimates, since it is notoriously difficult to appreciate the amount of shortening for those areas where (cryptic) deformation has been taken up –primarily- by diapir squeezing, salt rise and extrusion.

The way deformation is localized or transferred from the hinterland to the foreland also varies from the fold-and-thrust belt domain to the isolated minibasin province. In the fold-and-thrust belt, thrust wedge development responds to the critical taper theory (Dahlen, 1990): new thrusts form or former structures are reactivated to maintain the critical taper of the thrust wedge. Syncontractional sedimentation delays forward propagation of deformation since the orogenic wedge angle lowers with each syncontractional layer and more internal deformation is needed to reach the critical taper angle (Storti and McClay, 1995; Graveleau et al., 2012). The position of the deformation front is clearly constrained by syncontractional sedimentation (Pla et al., 2019), being more distal in the model without syncontractional sedimentation and more proximal in the model with high syncontractional sedimentation rate (Fig. 7a and c, respectively).

In our models, the taper angle abruptly diminished towards the

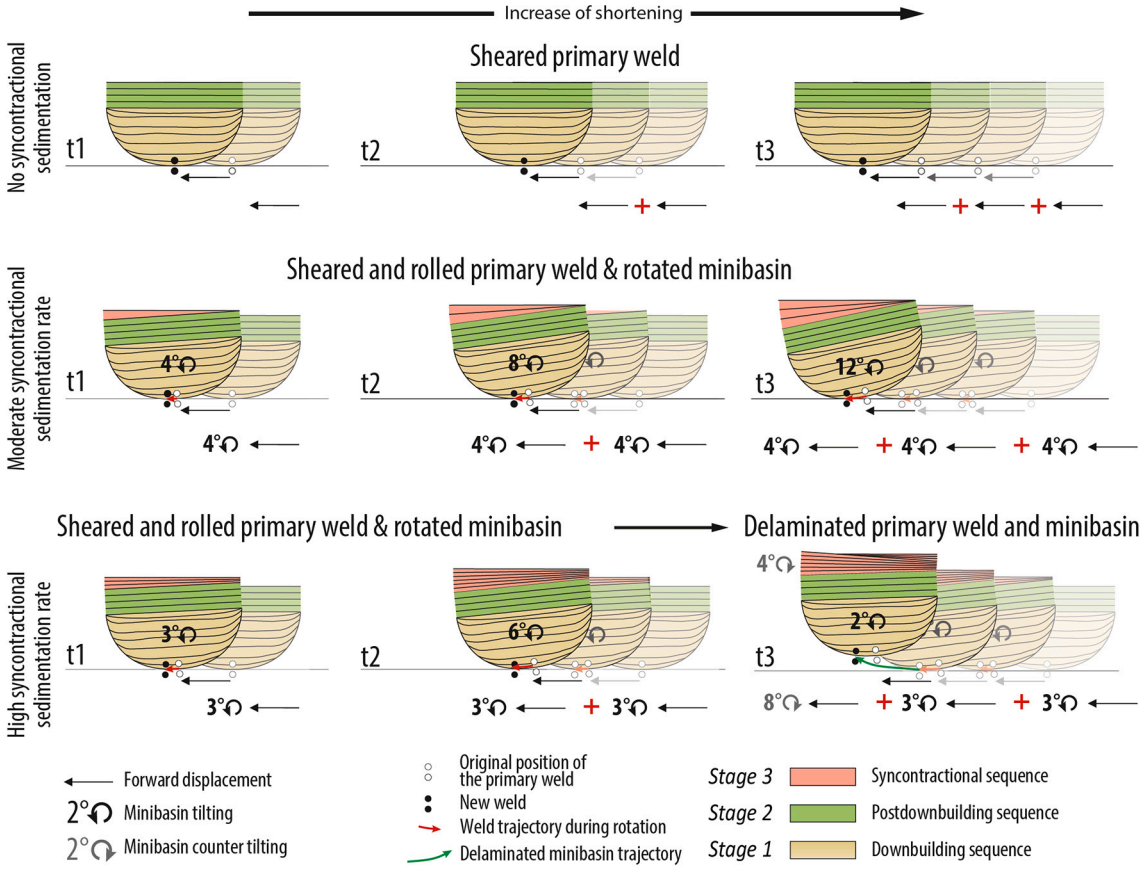

Fig. 14. Kinematic evolution during shortening (x axis) of sheared, rolled and delaminated primary welds and its relationship with minibasin tilting and syncontractional sedimentation rate (y axis). See text for further details.

isolated minibasin provinces. In that domain and as a general rule, deformation was broadly transferred forwards in a forward-stepping sequence. Exceptions are found. At the onset of deformation, mild deformation extends far from the moving backstop as evidenced by rejuvenation of distal diapirs (Figs. 4, 5). This implies that the model salt-sand package acts as a rigid beam that allowed for the transference of deformation towards distal areas, which is otherwise typical in sandbox analog models (Costa and Vendeville, 2002; Smit et al., 2003; Santolaria et al., 2015; Granado et al., 2017). This does not discard that further shortening concentrates in proximal salt walls and stocks. Besides, Out-of-sequence thrusting is common in salt-detached contractional systems. In our case, such activity is subordinate to the main forward-stepping sequence trend. Synchronous thrusting was commonly observed.

As pointed out by Rowan and Vendeville (2006) and Ferrer (2012), at the end of the contractional stage, contractional deformation extends across the isolated minibasin province even though salt diapirs are not completely closed (see Fig. 7). Since the closure and necking of salt bodies can accommodate a limited amount of shortening, secondary welding of proximal salt walls promotes the transfer of deformation to more distal salt walls by translation of juxtaposed minibasins along the basal model salt. This allows inferring that in these settings the forward transfer of deformation takes places through a framework of secondary welds (Fig. 10). Once again, this framework may be related to the pre-shortening configuration of the salt-sediment system. Stress transmission through the secondary welds framework would be analogous to the stress bridges developed in granular media (e.g. Gallagher et al., 1974). In addition, syncontractional sedimentation strengthens the overburden, and it becomes progressively harder for salt to rise and flare, so salt ridges may stay open longer, and shortening is then transferred outboard.

4.3. *Comparison to natural examples*

4.3.1. *The Fars Salient*

The Fars salt province of Zagros fold-and-thrust belt (Iran) forms a structural salient along the deformation front of the Zagros orogenic system (Sepehr and Cosgrove, 2004; Tavani et al., 2020; see Fig. 15a). The occurrence of this prominent salient, as observed in several other contractional fold-and-thrust belts (e.g. Muñoz et al., 2013; Izquierdo-Llavall et al., 2018), is attributed to a thicker sequence os Late Precambrian to Cambrian Hormuz evaporites which represent the regional *décollement* (e.g. Sepehr and Cosgrove, 2004; McQuarrie, 2004). On top of it, a 7–15 km thick, Paleozoic to Cenozoic sedimentary pile thickens towards the foreland (James and Wynd, 1965; Alavi, 2004).

The eastern Fars most outstanding feature (Fig. 15a) is a high concentration of extruding and buried diapirs cored by the Hormuz Salt (Trocmé et al., 2011). Salt bodies are largely recognized to predate the Late Cretaceous to Cenozoic Zagros orogeny (Callot et al., 2012). Strong supporting evidence for preorogenic diapirism are the Paleozoic and Mesozoic halokinetic sequences described from seismic and field observations (Edgell, 1996; Letouzey and Sherkati, 2004; Callot et al., 2007; Perotti et al., 2016; Stewart, 2018; Snidero et al., 2019, 2020). Shortening and squeezing of the eastern Fars diapirs resulted in a strong variability of the geometry and orientation of folds, often characterized by subordinate thrusts oblique to the main tectonic grain (see Fig. 15a). The structural style has been related to the presence of preexisting salt diapirs (e.g. Rowan and Vendeville, 2006; Jahani et al., 2009; Callot et al., 2012). Its presence is known to influence the structural spacing and the strike of structure and to deflect the trend of the fold limbs as

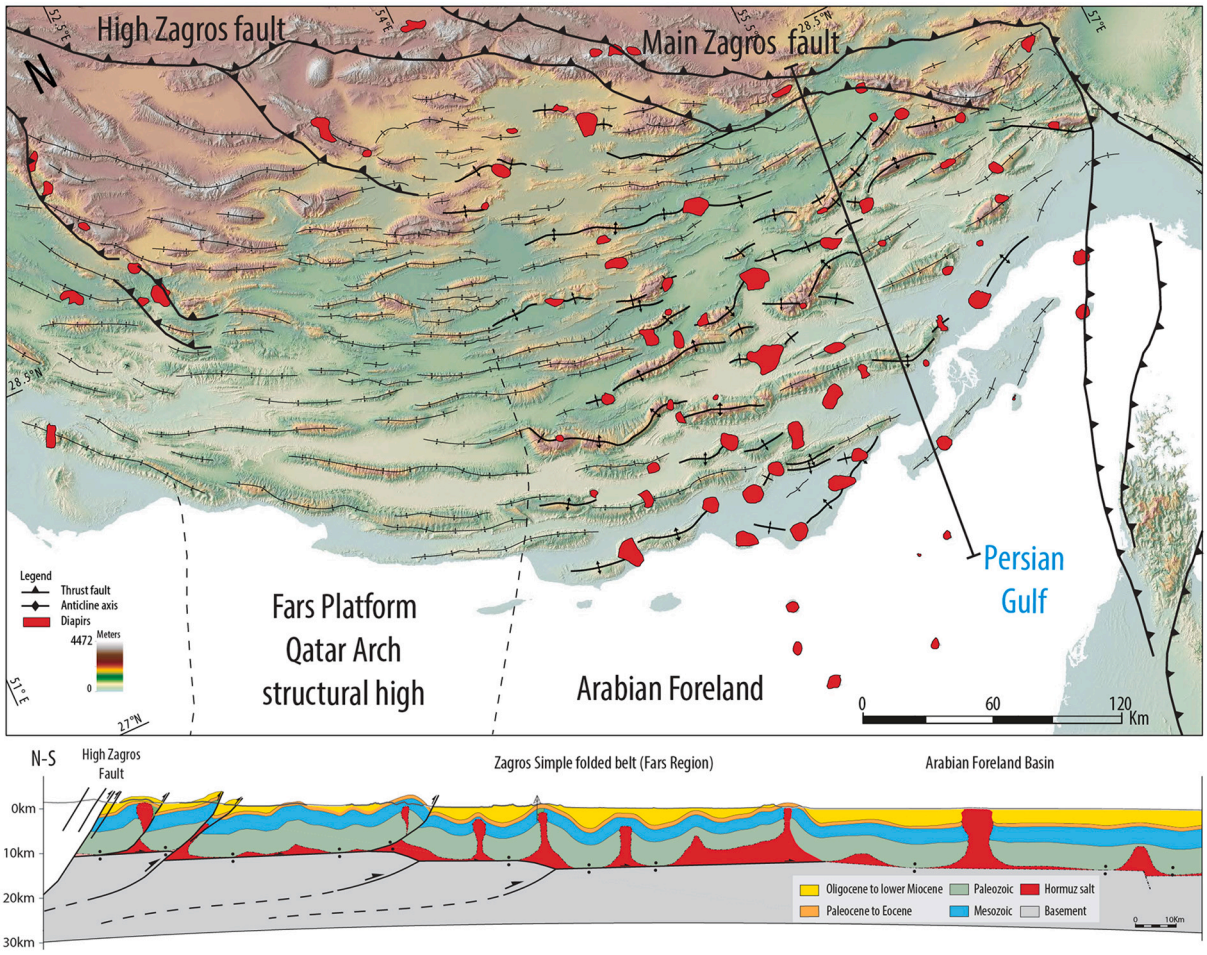

Fig. 15. a) Digital elevation model showing the major structural elements of the southeastern Zagros fold and thrust belt. Folds with a geometry and orientation influenced by the presence of the diapir location are highlighted. The basemap was created using the Shuttle Radar Topography Mission dataset (Farr et al., 2007). b) N-S regional cross-section of the eastern Fars region, modified after Tavakoli-Shirazi et al. (2013) and Snidero et al. (2019).

demonstrated by analog modeling experiments involving isolated diapirs (Dooley et al., 2009; Duffy et al., 2018; Santolaria et al., 2021).

Based on seismic data from the Persian Gulf and supported by analog modeling, Callot and coauthors (2012) pointed out Fars' salt stocks evolved from deep-seated salt ridges during the Mesozoic and Cenozoic. This implies that buried and currently extruding salt stocks are not isolated but connected through a framework of salt ridges or salt walls at depth (e.g., Snidero et al., 2019; Hassanpour et al., 2020). The salt stocks are suggested to be located at the junction of salt ridges as proposed for instance in the Pre-Caspian basin (Barde et al., 2002), and observed in analog modeling (Rowan and Vendeville, 2006; this study). Our experimental results stress the importance of the inherited pattern of salt ridges as a first order controlling factor for the obliquity of contractional structures. Thus, we suggest that the structural pattern observed in the eastern Fars area resulted from of 1) the precontractional distribution of salt walls or ridges in combination with 2) structures related to salt stock squeezing.

In the western sector of the Fars Salient, almost no diapirs crop out. The transition between these two areas coincides with the eastern limit of the Qatar Arch structural high. (Fig. 15a). The western Fars structures are characterized by folds, tens to hundred-kilometer long, regularly spaced and trending nearly perpendicular to the shortening direction (Agard et al., 2005; McQuarrie, 2004). The change in the structural style is associated with the thinning of the Hormuz Salt towards the Qatar Arch structural high (Bahroudi and Talbot, 2003; Perotti et al., 2011). The role and characteristics of this transition has been previously investigated through different analog modeling setups. In each case, a thick salt domain was used in order to model the eastern Fars, where i) Bahroudi and Koyi (2003) do not consider preexisting diapirs and set an abrupt transition to a frictional detachment and ii) Callot et al. (2012) considered preexisting diapirs and a progressive thinning towards the Qatar Arch structural high analog. The detachment rheology transition in Bahroudi and coauthors' experiment led to the formation of a salt-bearing, low taper angle fold belt salient on top of the *décollement* and a higher taper angle thrust wedge in the frictional detachment area. These contrasting structural styles were separated by strike slip fault as the ones interpreted to limit the Fars Platform (Husseini, 1988; Hessami et al., 2001). In Callot and coauthors' model, the progressive thinning of the salt-equivalent layer resulted in a gradual decrease of the structural spacing. Besides, the addition of preexisting diapirs led to the occurrence of short, wide and sinuous structures, a closer analog to the eastern Fars area. As observed in our models and in agreement with those of Callot et al. (2012), the presence of the observed diapirs is explained by the existence of a thick enough the Hormuz Salt unit which allowed the formation of the salt-sediment system (see Section 3.1). However, in Bahroudi and Koyi's (2003) and Callot and coauthors (2012) models, an excessive thinning of the salt-equivalent layer resulted in a less effective *décollement*, entailing the formation of a reentrant. This contradicts what it is observed in the Fars Salient deformation front where no reentrant exists. This suggests that, although thinner, the Hormuz Salt still acts as an effective *décollement* above the Fars Platform.

Similarities with the Fars Salient also exist in terms of shortening and sedimentary rates. The presented cross-section (Fig. 15b) implies a 13.7% of total shortening mainly accumulated over the last 30 Myr, with

an average syncontractional depositional rate of 34 m/Ma in the Persian Gulf (Perotti et al., 2016) and over 2 km of synfolding sediments deposited on-shore. This ratio is equivalent to the high syncontractional sedimentary rate of our modeling, exceeding the 0.8 to 2 mm/h threshold that hampered the minibasin rotation. In fact, the analog modeling results of model 4 (Fig. 9), match significantly well the attained values of the Fars minibasin tilting (Fig. 15b).

4.3.2. The Northern Calcareous Alps

The Northern Calcareous Alps are a N-to NW-directed salt-detached fold-and-thrust belt belonging to the European Alpine orogenic system (Linzer et al., 1997). The fold-and-thrust belt is characterized by multiple structural orientations, large, overturned panels, geological contacts either omitting or repeating stratigraphy and sudden changes on fold-wavelength associated with stratigraphic thickness changes (Granado et al., 2019); all these features are systematically associated with the existence of a Permian-Triassic layered evaporitic sequence at the bottom of the deformed succession of Triassic-Jurassic carbonates (Fig. 16a). One remarkable example is represented by the Gamsstein minibasin (Fig. 16b). Erosional levelling and large tilting (ca. 45° to the NW) provide an almost unique example of the cross-sectional view of a bowl-shaped Middle-Upper Triassic carbonate minibasin sunk into a thick layer of salt (Strauss et al., 2020). The Gamsstein minibasin and its flanking salt structures were later incorporated on the Northern Calcareous Alps fold-and-thrust belt with the onset of convergence by about Middle-Late Jurassic times (Granado et al., 2019). The northern boundary of the minibasin is marked by a subtractive contact that juxtaposes *syn*-orogenic Cretaceous strata on the hanging wall to Middle Triassic strata on the footwall; the contact is however characterized by strong compressional fabrics. In comparison, further east in the Northern Calcareous Alps typical hanging wall flats on footwall ramps relationships are observed, bringing older on younger stratigraphy (Fig. 16a, c) such as in other well-known fold-and-thrust belts (Boyer and Elliot, 1982). Detailed geological mapping of the area (Schnabel et al., 2002) shows similar changes in stratigraphic thickness and stratigraphic omissions to those reported from around the Gamsstein minibasin, as well as the presence of salt soling thrust sheets. Given the scarcity of exploration wells in the Northern Calcareous Alps, the construction of cross-sections entails significant uncertainty; here, we use sandbox models as structural-stratigraphic templates to reduce it.

Both illustrated sections display markedly different structural relationships: whereas the Gamsstein minibasin shows a significant foreland-ward tilting of about 45°, the eastern section displays a rather typical hinterland-dipping imbricate fan of thrusts. The cause(s) for the NW-tilting of the Gamsstein minibasin (Fig. 16b) are still unclear: tilting could have occurred during the passive margin stage as a result of salt-detached extension, however no stratigraphic record for that tilting in the form of roll-over wedges has been found within the Gamsstein

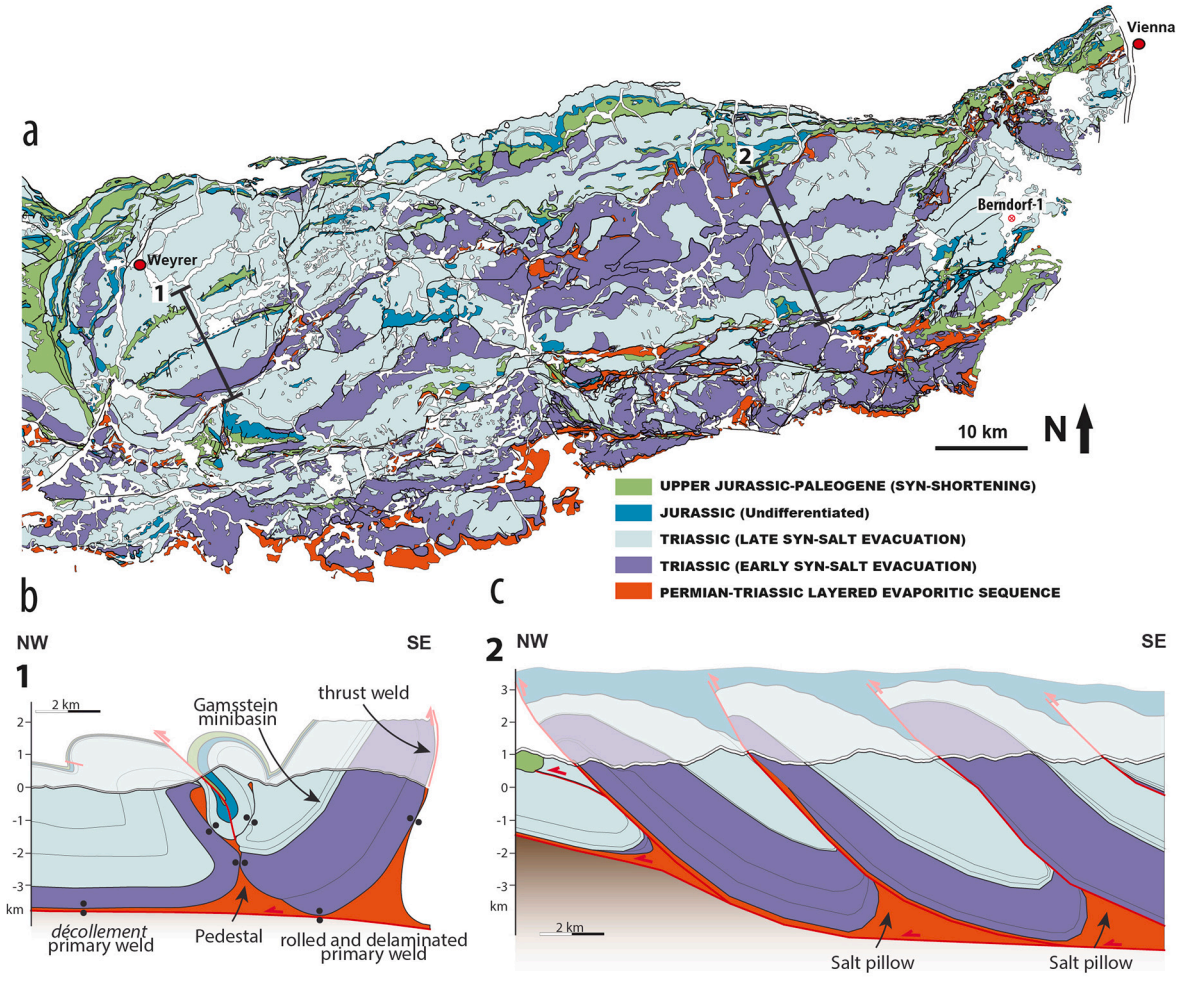

Fig. 16. a) Geological map of the study area based on the 1:200.000 geological map of Niederösterreich (Lower Austria) modified from Schnabel et al. (2002). b) NW–SE cross-section; note the contact omitting stratigraphy juxtaposing Cretaceous syn-shortening strata on the hanging wall to Middle Triassic early syn-downbuilding series (modified from Granado et al., 2019). C) NW–SE cross-section showing hanging wall flats on footwall ramps geometries, involving a stratigraphy with marked changes in depositional stratigraphic thickness. Depth to basal *décollement* is constrained by the nearest well Berndorf _1 that reached crystalline basement at >6000 m TVD (Wachtel and Wessely, 1981).

minibasin. On the contrary, analog modeling suggests that loading by syncontractional growth strata may contribute to tilting (up to 20°), but large erosion has reduced growth strata preservation to a minimum around the Gamsstein minibasin (Schnabel et al., 2002), shedding no light into this. Our modeling additionally suggests that forward tilting can relate to shortening and translation, including back-thrusting along secondary welds, leading to décollement, rolling and delamination of primary welds (Fig. 14), in a way similar to what has been described in the Sivas Basin, for instance (Kergaravat et al., 2016; Legeay et al., 2019). Other mechanisms that have not been considered in our modeling but that can potentially be responsible for the observed tilting of minibasins in fold-and-thrust belts in general are the late involvement of the presalt basement by thick-skinned shortening (Dooley and Hudec, 2020), and/or the presence of hinterland-dipping basement steps acting as ramps during salt-detached contraction (Granado et al., 2021). In the case of the eastern cross-section (Fig. 16c), the main uncertainty relates to the shape of the footwalls; to address this uncertainty we have used the results of models Model 2 (Fig. 9), where salt pillows nucleated a series of forward-breaking thrusts bringing older stratigraphy onto younger stratigraphy.

The analog modeling results presented here match significantly well with the regional map patterns of the Northern Calcareous Alps (Schnabel et al., 2002), where strained stripes of evaporites and related rocks such as *rauhwacken* (see Warren, 2016 p. 656) have been recently interpreted to rather relate to the squeezing, jostling and secondary welding and thrust welding between closely juxtaposed isolated minibasins (Granado et al., 2019, 2021; Strauss et al., 2020). Upon orogenic convergence, and contraction of the salt network, all inherited complexities have promoted overly complicated tectonic histories when viewed without an eye for salt tectonics.

5. Conclusions

The evolution of a salt-sediment system depends on the original thickness and distribution of salt deposits. For those contractional systems where *décollement* horizons root in salt, the preshortening configuration of the salt-sediment system exerts a primary control on subsequent contraction. As shown by our modeling, that rapid changes on structural styles develop from originally thin to thick salt areas. Isolated-minibasin provinces show contractional features mimicking the inherited salt ridges pattern at the end of downbuilding; on the other hand, thrusting nucleates at salt pillow apexes, where the original salt deposits are thinner. Finally, a linear fold-and-thrust belt develops where the salt deposits were thinnest. Hence, a broad along-strike spectrum of structures from salt-related to thrust wedge-related occur; there is no need to invoke abrupt thickness changes in the basal salt layer, or basement features, to explain sudden changes in the along-strike structural style of the fold-belt. Apparent strike-slip motions may be confused when dealing with closely juxtaposed minibasins bound by sub-vertical secondary welds.

Contractional deformation transports minibasins forward, coinciding with the reactivation and progressive squeezing of the bounding salt ridges, until they become secondarily welded. Welded salt ridges led to the formation of a secondary weld framework that permits deformation transfer towards the foreland, entailing forward displacement of colliding minibasins and shearing of primary welds.

Where model salt was originally thin, syncontractional sedimentation prevents rapid forward propagation of thrusting, increases the wavelength of structures and the fault displacement. On the contrary, where model salt was originally thick, syncontractional sedimentation promotes the rotation of minibasins around a horizontal axis normal to the shortening direction. Also, in these domains, syncontractional sedimentation prevents forward propagation of the deformation Forward minibasins rotation entails migration of the original primary weld (i.e. rolled primary weld), backthrusting, as well as development of growth strata geometries in the syncontractional sediments. A substantial increment of syncontractional sedimentation rate, which better distributes the sedimentation and decreases sedimentary load differences, slows down minibasins tilting, whereas delaminated minibasins and related delaminated welds developed.

Some of the assertions above may seem rather obvious; however, these principles are fundamental to understand the structural complexity of many fold-and-thrust belts. Still, it is in the common knowledge that different structural orientations relate to different orogenic events with differing contractional directions, or to large strike-slip tectonics. Some of the principles stated on this work also set base for harmonizing structural and stratigraphic development. The physical analogue models presented in this work provide a better understanding of the geometries, kinematics (and mechanics) of fold-and-thrust belts. The models can be used to predict the presence of subtle stratigraphic, structural and mixed mode traps, provide insights for seismic data interpretation around salt diapirs, and derisk trap configuration.

Supplementary data to this article can be found online at https://doi.org/10.1016/j.tecto.2021.229078.

CRediT authorship contribution statement

P. Santolaria: Conceptualization, Methodology, Investigation, Writing – original draft, Writing – review & editing. **P. Granado:** Writing – review & editing. **N. Carrera:** Conceptualization, Methodology, Investigation, Writing – original draft. **C.L. Schneider:** Writing – review & editing. **O. Ferrer:** Writing – review & editing. **M. Snidero:** Writing – review & editing. **P. Strauss:** Writing – review & editing. **K. Pelz:** Writing – review & editing. **E. Roca:** Writing – review & editing. **J. A. Muñoz:** Supervision, Conceptualization, Writing – review & editing.

Declaration of Competing Interest

The authors declare that they have no known competing financial interests or personal relationships that could have appeared to influence the work reported in this paper.

Acknowledgements

This is a contribution of the Institut de Recerca Geomodels and the Grup de Geodinàmica i Anàlisi de Conques (2014SGR-467) from the Universitat de Barcelona. This research was primarily funded by ConocoPhillips (USA) and supported by the project "Tectónica Salina en Cinturones Contractivos" (SALTCONBELT- CGL2017-85532-P), funded by Agencia Estatal de Investigación (AEI) and Fondo Europeo de Desarrollo Regional (FEDER). PG was financially supported by OMV Exploration and Production GmbH through the Fundaciò Bosch i Gimpera. The experimental program was executed at the GEOMODELS Analogue Modelling Laboratory at the University of Barcelona supported by a Scientific Infrastructure grant (UNBA08-4E-006) provided by the European Regional Development Fund of the Ministerio de Ciencia e Innovación of the Spanish Government and Statoil (now Equinor). Petroleum Experts are also acknowledged for providing Move software. Finally, we thank Jean P. Callot and Tim Dooley for constructive revisions that helped us to improve the manuscript.

References

Adam, J., Urai, J., Wieneke, B., Oncken, O., Pfeiffer, K., Kukowski, N., Lohrmann, J., Hoth, S., van der Zee, W., Schmatz, J., 2005. Shear localisation and strain distribution during tectonic faulting—new insights from granular-flow experiments and high-resolution optical image correlation techniques. J. Struct. Geol. 27, 283–301.

Agard, P., Omrani, J., Jolivet, L., Mouthereau, F., 2005. Convergence history across Zagros (Iran): constraints from collisional and earlier deformation. Int. J. Earth Sci. 98, 401–419. https://doi.org/10.1007/s00531-005-0481-4.

Alavi, M., 2004. Regional stratigraphy of the Zagros Fold-Thrust Belt of Iran and its proforeland evolution. Am. J. Sci. 304, 1–20.

Bahroudi, A., Koyi, H., 2003. The effect of spatial distribution of Hormuz salt on deformation style in the Zagros fold and thrust belt: an analogue modeling approach. J. Geol. Soc. London 160, 719–733.
Bahroudi, A., Talbot, C.J., 2003. The configuration of the basement beneath the Zagros Basin. J. Pet. Geol. 26 (3), 257–282.
Barde, J.P., Gralla, P., Harwijanto, J., Marsky, J., 2002. Exploration at the eastern edge of the Precaspian basin: impact of data integration on upper Permian and Triassic prospectivity. AAPG Bull. 86, 399–415.
Boyer, S.R., Elliot, D., 1982. Thrust systems. Am. Assoc. Pet. Geol. Bull. 66, 1196–1230.
Callot, J.P., Jahani, S., Letouzey, J., 2007. The role of pre-existing diapirs in fold and thrust belt development. In: Lacombe, O., Lavé, J., Roure, F., Verges, J. (Eds.), Thrust Belts and Foreland Basins: from Fold Kinematics to Hydrocarbon Systems, pp. 309–326.
Callot, J.P., Trocmé, V., Letouzey, J., Albouy, E., Jahani, S., Sherkati, S., 2012. Pre-existing salt structures and the folding of the Zagros Mountains. In: Alsop, G.I., Archer, S.G., Hartley, A.J., Grant, N.T., Hodgkinson, R. (Eds.), Salt Tectonics, Sediments and Prospectivity, Geol. Soc. Lond., Spec. Publ., 363, pp. 545–561. https://doi.org/10.1144/SP363.27.
Callot, J.P., Salel, J.F., Letouzey, J., Daniel, J.M., Mengus, J.M., Pillot, D., Ringenbach, J. C., 2016. Three-dimensional evolution of salt controlled minibasins: interactions, folding and megaflap development. Am. Assoc. Pet. Geol. Bull. 100, 1419–1442.
Calvín, P., Casas-Sainz, A.M., Villalaín, J.J., Moussaid, B., 2018. Extensional vs. compressional deformation in the Central High Atlas salt province: a paleomagnetic approach. Tectonophysics 734-735, 130–147. https://doi.org/10.1016/j.tecto.2018.04.007.
Costa, E., Vendeville, B.C., 2002. Experimental insights on the geometry and kinematics of fold-and-thrust belts above a weak, viscous evaporite décollement. J. Struct. Geol. 24 (11), 1729–1739.
Couzens-Schultz, B.A., Vendeville, B.C., Wiltschko, D.V., 2003. Duplex style and triangle zone formation: insights from physical modeling. J. Struct. Geol. 25, 1623–1644.
Dahlen, F.A., 1990. Critical taper model of fold-and-thrust belts and accretionary wedges. Annu. Rev. Earth Planet. Sci. 18, 55–99.
Dell'Ertole, D., Schellart, W.P., 2013. The development of sheath folds in viscously stratified materials in simple shear conditions: an analogue approach. J. Structural Geool. 56, 129–141.
Dooley, T., Jackson, M.P.A., Hudec, M.R., 2013. Coeval extension and shortening above and below salt canopies on an uplifted, continental margin: application to the northern Gulf of Mexico. AAPG Bull. 97, 1737–1764.
Dooley, T., Duffy, O., Hudec, M., Fernandez, N., 2019. Shortening of Diapir Provinces: Translation, Tilting and Rotation of Minibasins in Isolated Minibasin Systems (Search and Discovery Article #11229).
Dooley, T.P., Hudec, M.R., 2020. Extension and inversion of salt-bearing rift systems. Solid Earth 11, 1187–1204. https://doi.org/10.5194/se-11-1187-2020.
Dooley, T.P., Jackson, M.P.A., Hudec, M.R., 2009. Inflation and deflation of deeply buried salt stocks during lateral shortening. J. Struct. Geol. 31, 582–600. https://doi.org/10.1016/j.jsg.2009.03.013.
Duffy, O.B., Fernandez, N., Hudec, M.R., Jackson, M.P.A., Burg, G., Dooley, T.P., Jackson, C.A.L., 2017. Lateral mobility of minibasins during shortening: insights from the SE Precaspian Basin, Kazakhstan. J. Struct. Geol. https://doi.org/10.1016/j.jsg.2017.02.002.
Duffy, O.B., Dooley, T.P., Hudec, M.R., Jackson, M.P.A., Fernandez, N., Jackson, C.A.L., Soto, J.I., 2018. Structural evolution of salt-influenced fold-and-thrust belts: a synthesis and new insights from basins containing isolated salt diapirs. J. Struct. Geol. 114, 206–221.
Duffy, O.B., Dooley, T.P., Hudec, M.R., Fernández, N., Jackson, C.A.-L., Soto, J.I., 2021. Principles of shortening in salt basins containing isolated minibasins. Basin Res. 33 (3), 2089–2117. https://doi.org/10.1111/bre.12550.
Edgell, H.S., 1996. Salt tectonics in the Persian Gulf basin, in Salt Tectonics. In: Alsop, G. L., Blundell, D.L. (Eds.), Geol. Soc. Spec. Publ. 100, 129–151. https://doi.org/10.1144/GSL.SP.1996.100.01.10.
Farr, T.G., Rosen, A.P., Caro, E., Crippen, R., Duren, R., Hensley, S., Kobrick, M., Paller, M., Rodriguez, E., Roth, L., Seal, D., Shaffer, S., Shimada, J., Umland, J., Werner, M., Oskin, M., Burbank, D., Alsdorf, D., 2007. The shuttle radar Topography mission. Rev. Geophys. 45 https://doi.org/10.1029/2005RG000183.
Ferrer, O., 2012. Salt tectonics in the Parentis Basin (eastern Bay of Biscay). PhD thesis. University of Barcelona (291 pp.).
Ferrer, O., Gratacós, O., Roca, E., Muñoz, J.A., 2017. Modeling the interaction between presalt seamounts and gravitational failure in salt-bearing passive margins: the Messinian case in the northwestern Mediterranean Basin. Interpretation 5, 99–117.
Gallagher, J.J., Friedman, M., Handin, J., Sowers, G.M., 1974. Experimental studies relating to microfracture in sandstone. Tectonophysics 2, 203–247.
Granado, P., Urgeles, R., Sábat, F., Albert-Villanueva, E., Roca, E., Muñoz, J.A., Mazzucca, N., Gambini, R., 2016. Geodynamical framework and hydrocarbon plays of a salt giant: the North Western Mediterranean Basin. Pet. Geosci. 22, 309–321. https://doi.org/10.1144/petgeo2015-084.
Graham, R., Jackson, M., Pilcher, R., Kilsdonk, B., 2012. Allochthonous salt in the sub-Alpine fold–thrust belt of Haute Provence, France. In Salt tectonics, sediments and prospectivity. Geolog. Soc. London Spec. Pub. 363, 595–615. https://doi.org/10.1144/SP363.30.
Granado, P., Ferrer, O., Muñoz, J.A., Thöny, W., Strauss, P., 2017. Basin inversion in tectonic wedges: insights from analog modeling and the Alpine-Carpathian fold-and-thrust belt. Tectonophysics 703–704, 50–68.
Granado, P., Roca, E., Strauss, P., Pelz, K., Muñoz, J.A., 2019. Structural styles in fold-and-thrust belts involving early salt structures: the Northern Calcareous Alps (Austria). Geology 47 (1), 51–54. https://doi.org/10.1130/G45281.1.
Granado, P., Ruh, J.B., Santolaria, P., Strauss, P., Muñoz, J.A., 2021. Stretching and contraction of extensional basins with pre-rift salt: a numerical modeling approach. Front. Earth Sci. 9, 648937. https://doi.org/10.3389/feart.2021.648937.
Graveleau, F., Malavieille, J., Dominguez, S., 2012. Experimental modeling of orogenic wedges: a review. Tectonophysics 538-540, 1–66.
Harrison, J., Jackson, M., 2014. Exposed evaporite diapirs and minibasins above a canopy in Central Sverdrup Basin, Axel Heiberg Island, Arctic Canada. Basin Res. 26, 567–596.
Hassanpour, J., Yassaghi, A., Muñoz, J.A., Jahani, S., 2020. Salt tectonics in a double salt-source layer setting (Eastern Persian Gulf, Iran): Insights from interpretation of seismic profiles and sequential cross-section restoration. Basin Res. https://doi.org/10.1111/bre.12459.
Hessami, K., Koyi, H.A., Talbot, C.J., 2001. The significant of strike–slip faulting in the basement of Zagros fold and thrust belt. J. Pet. Geol. 24, 5–28.
Hubbert, M.K., 1951. Mechanical basis for certain familiar geologic structures. Geol. Soc. Am. Bull. 62 (2), 355.
Husseini, M.I., 1988. The Arabian Infracambrian extensional system. Tectonophysics 148, 93–103.
Izquierdo-Llavall, E., Roca, E., Xie, H., Pla, O., Muñoz, J.A., Rowan, M.G., Yuan, N., Huang, S., 2018. Influence of overlapping décollements, syntectonic sedimentation, and structural inheritance in the evolution of a contractional system: the central Kuqa fold-and-thrust belt (Tian Shan Mountains, NW China). Tectonics 37, 2608–2632. https://doi.org/10.1029/2017TC004928.
Jackson, A.-L., Duffy, O.B., Fernandez, N., Dooley, T.P., Hudec, M.R., Jackson, P.A., Burg, G., 2019. The stratigraphic record of minibasin subsidence, Precaspian Basin, Kazakhstan. Basin Res. 32 (4), 1–25. https://doi.org/10.1111/bre.12393.
Jackson, M.P., Hudec, M.R., 2017. Salt Tectonics: Principles and Practice. Cambridge University Press, Cambridge (498 pp.).
Jackson, M.P.A., Harrison, J.C., 2006. An allochthonous salt canopy on Axel Heiberg Island. Sverdrup basin, Arctic Canada: Geol. 34, 1045–1048.
Jackson, M.P.A., Hudec, M.R., Jennette, D.C., Kilby, R.E., 2008. Evolution of the Cretaceous Astrid thrust belt in the ultradeep-water Lower Congo basin, Gabon. AAPG Bull. 92, 487–511.
Jackson, M.P.A., Dooley, T.P., Hudec, M.R., McDonnell, A., 2011. The Pillow Fold belt: A Key Subsalt Structural Province in the northern Gulf of Mexico: AAPG Search and Discovery article 10329 (21 p.), accessed March 31, 2021. http://www.searchanddiscovery.com/pdfz/documents/2011/10329jackson/ndx_jackson.pdf.html.
Jahani, S., Callot, J.P., Letouzey, J., Frizon de Lamotte, D., Leturmy, P., 2007. The salt plug of the eastern Fars province (Zagros, Iran): A brief outline of their past and present activity. In: Lacombe, O., Lave, J., Roure, F., Verges, J. (Eds.), Thrust Belts and Fore- land Basins: from Fold Kinematics to Hydrocarbon Systems. Springer, Berlin, pp. 289–308.
Jahani, S., Callot, J.P., Letouzey, J., Frizon de Lamotte, D., 2009. The eastern termination of the Zagros fold and thrust belt (Iran): relationship between salt plugs, folding and faulting. Tectonics 28, TC6004. https://doi.org/10.1029/2008TC002418.
James, G.A., Wynd, J.G., 1965. Stratigraphic nomenclature of Iranian oil consortium agreement area. AAPG Bull. 49 (12), 2182–2245.
Kergaravat, C., Ribes, C., Legeay, E., Callot, J.P., Kavak, K.S., Ringenbach, J.C., 2016. Minibasins and salt canopy in foreland fold-and-thrust belts: the Central Sivas Basin, Turkey. Tectonics 35. https://doi.org/10.1002/2016TC004186.
Konstantinovskaya, E., Malavieille, J., 2011. Thrust wedges with décollement levels and syntectonic erosion: a view from analogue models. Tectonophysics 502, 336–350.
Legeay, E., Ringenbach, J.-C., Kergaravat, C., Pichat, A., Mohn, G., Vergés, J., Sevki Kavak, K., Callot, J.-P., 2019. Structure and kinematics of the Central Sivas Basin (Turkey): Salt deposition and tectonics in an evolving fold and thrust belt. In: Hammerstein, J.A., Di Cuia, R., Cottam, M.A., Zamora, G., Butler, R.W.H. (Eds.), Fold and Thrust Belts: Structural Style. Geological Society, London, Special Publications, Evolution and Exploration, p. 490. https://doi.org/10.1144/SP490-2019-92.
Letouzey, J., Sherkati, S., 2004. Salt movement, tectonic events, and structural style in the central Zagros fold and thrust belt (Iran). In: Post, P.J., Olson, D.L., Lyons, K.T., Palmes, S.L., Harrison, P.F., Rosen, N.C. (Eds.), Salt–Sediment Interactions and Hydrocarbon Prospectivity: Concepts, Applications, and Case Studies for the 21st Century, 24th Annual Research Conference. SEPM Foundation, pp. 444–463.
Linzer, H.G., Moser, F., Nemes, F., Ratschbacher, L., Sperner, B., 1997. Buildup and dismembering of the eastern Northern Calcareous Alps. Tectonophysics 272, 97–124. https://doi.org/10.1016/S0040-1951(96)00254-5.
Lohrmann, J., Kukowski, N., Adam, J., Oncken, O., 2003. The impact of analogue material properties on the geometry, kinematics, and dynamics of convergent sand wedges. J. Struct. Geol. 25 (10), 1691–1711.
McQuarrie, N., 2004. Crustal scale geometry of the Zagros fold–thrust belt, Iran. J. Struct. Geol. 26, 519–535.
Moretti, I., Callot, J.-P., Principaud, M., Pillot, D., 2013. Salt pillows and localization of early structures: case study in the Ucayali Basin (Peru). Geol. Soc. Lond., Spec. Publ. 377, 43–58.
Muñoz, J.A., Beamud, E., Fernández, O., Arbués, P., Dinarès-Turell, J., Poblet, J., 2013. The Ainsa Fold and Thrust Oblique Zone of the Central Pyrenees: kinematics of a curved contractional system from paleomagnetic and structural data. Tectonics 32, 1142–1175.
Nilsen, K.T., Vendeville, B.C., Johansen, J.T., 1995. Influence of regional tectonics on halokinesis in the Nordkapp Basin, Barents Sea. In: Jackson, M.P.A., Roberts, D.G., Snelson, S. (Eds.), Salt Tectonics: A Global Perspective: AAPG Memoir, vol. 65, pp. 413–436.
Perotti, C., Carruba, S., Rinaldi, M., Bertozzi, G., Feltre, L., Rahimi, M., 2011. The Qatar–South Fars Arch Development (Arabian Platform, Persian Gulf): insights from

seismic interpretation and analogue modelling. In: Schattner, U. (Ed.), New Frontiers in Tectonic Research - at the Midst of Plate Convergence. InTech, pp. 325–352.
Perotti, C., Chiariotti, L., Bresciani, L., Cattaneo, L., Toscani, G., 2016. Evolution and timing of salt diapirism in the Iranian sector of the Persian Gulf. Tectonophysics 679, 180–198.
Pla, O., Roca, E., Xie, H., Izquierdo-Llavall, E., Muñoz, J.A., Rowan, M.G., et al., 2019. Influence of syntectonic sedimentation and décollement rheology on the geometry and evolution of orogenic wedges: Analog modeling of the Kuqa fold-and-thrust belt (NW China). Tectonics 38, 2727–2755. https://doi.org/10.1029/2018TC005386.
Roma, M., Vidal-Royo, O., McClay, K., Ferrer, O., Muñoz, J.A., 2018. Tectonic inversion of salt-detached ramp-syncline basins as illustrated by analog modeling and kinematic restoration. Interpretation 6 (1), T127–T144.
Rowan, M.G., Ratliff, R.A., 2012. Cross-section restoration of salt-related deformation: best practices andpotential pitfalls. J. Struct. Geol. 41, 24–37. https://doi.org/10.1016/j.jsg.2011.12.012.
Rowan, M.G., Vendeville, B.C., 2006. Foldbelts with early salt withdrawal and diapirism: physical model and examples from the northern Gulf of Mexico and the Flinders Ranges, Australia. Mar. Pet. Geol. 23 (9–10), 871–891.
Rowan, M.G., Weimer, P., 1998. Salt sediment interaction, northern Green Canyon and Ewing bank (offshore Louisiana), northern Gulf of Mexico. AAPG Bull. 82, 1055–1082.
Rowan, M.G., Vendeville, B.C., Peel, F.J., 2004. Gravity-driven Fold Belts on Passive margins. In: McClay, K.R. (Ed.), Thrust Tectonics and Hydrocarbon Systems, AAPG Memoir, vol. 82, pp. 157–182.
Santolaria, P., Vendeville, B.C., Graveleau, F., Soto, R., Casas-Sainz, A.M., 2015. Double evaporitic décollements: influence of pinch-out overlapping in experimental thrust wedges. J. Struct. Geol. 76, 35–51.
Santolaria, P., Ferrer, O., Rowan, M.G., Snidero, M., Carrera, N., Granado, P., Muñoz, J. A., Roca, E., Schneider, C.L., Piña, A., Zamora, G., 2021. Influence of preexisting salt diapirs during thrust wedge evolution and secondary welding: insights from analog modeling. J. Struct. Geol. 149, 104374. https://doi.org/10.1016/j.jsg.2021.104374.
Schellart, W.P., 2000. Shear test results for cohesion and friction coefficients for different granular materials: scaling implications for their usage in analogue modelin. Tectonophysics 324, 1–16. https://doi.org/10.1016/S0040-1951(00)00111-6.
Schnabel, W., Fuchs, G., Matura, A., Bryda, G., Egger, J., Krenmayer, H.G., Mandl, G., Nowotny, A., Rotzel, R., Scharbert, S., 2002. Geologische Karte von Niederösterreich, 3B1: Vienna, Geological Survey of Austria (GBA), 2 Sheets (scale 1: 200,000).
Sepehr, M., Cosgrove, J.W., 2004. Structural framework of the Zagros fold–thrust belt. Iran. Mar. Pet. Geol. 21 (7), 829–843. https://doi.org/10.1016/j.marpetgeo.2003.07.006.
Smit, J.H.W., Brun, J.P., Soukoutis, D., 2003. Deformation of brittle–ductile thrust wedges in experiments and nature. J. Geophys. Res. 108 (B10), 2480. https://doi.org/10.1029/2002JB002190.
Snidero, M., Muñoz, J.A., Carrera, N., Butillé, M., Mencos, J., Motamedi, H., Piryaei, A., Sàbat, F., 2019. Temporal evolution of the Darmadan salt diapir, eastern Fars region, Iran. Tectonophysics 766, 115–130.
Snidero, M., Carrera, N., Mencos, J., Butillé, M., Granado, P., Tavani, S., López-Mir, B., Sàbat, F., Muñoz, J.A., 2020. Diapir kinematics in a multi-layer salt system from the eastern Persian Gulf. Mar. Pet. Geol. 117, 104402. https://doi.org/10.1016/j.marpetgeo.2020.104402.
Sommaruga, A., 1999. Décollement tectonics in the Jura foreland fold-and-thrust belt. Mar. Pet. Geol. 16, 111–134.
Stewart, S.A., 2018. Hormuz salt distribution and influence on structural style in NE Saudi Arabia. Petrol. Geosci. 24, 143–158. https://doi.org/10.1144/petgeo2017-011.
Storti, F., McClay, K., 1995. Influence of syntectonic sedimentation on thrust wedges in analog models. Geology 23 (11), 999–1002.
Strauss, P., Granado, P., Muñoz, J.A., 2020. Subsidence analysis of salt tectonics-driven carbonate minibasins (Northern Calcareous Alps, Austria). Basin Res. https://doi.org/10.1111/bre.12500.
Tavakoli-Shirazi, S., Frizon de Lamotte, D., Wrobel-Daveau, J.-C., Ringenbach, J.-C., 2013. Pre-Permian uplift and diffuse extensional deformation in the High Zagros Belt (Iran): integration in the geodynamic evolution of the Arabian plate. Arab. J. Geosci. 6 (7), 2329–2342. https://doi.org/10.1007/s12517-012-0542-5.
Tavani, S., Camanni, G., Nappo, M., Snidero, M., Ascione, A., Valente, E., Gharabeigli, G., Morsalnejad, D., Mazzoli, S., 2020. The Mountain Front Flexure in the Lurestan region of the Zagros belt: Crustal architecture and role of structural inheritances. J. Struct. Geol. 135, 104022. https://doi.org/10.1016/j.jsg.2020.104022.
Trocmé, V., Albouy, E., Callot, J.P., Letouzey, J., Rolland, N., Goodarzi, H., Salman, J., 2011. 3D structural modelling of the southern Zagros fold-and-thrust belt diapiric province. Cambridge University Press 148 (5–6), 879–900. https://doi.org/10.1017/S0016756811000446.
Trusheim, F., 1960. Mechanism of salt migration in northern Germany. Am. Assoc. Pet. Geol. Bull. 44, 1519–1540.
Vendeville, B.C., 2002. A new interpretation of Trusheim's classic model of salt-diapir growth. Gulf Coast Assoc. Geol. Soc. Trans. 52, 943–952.
Wachtel, V.G., Wessely, G., 1981. Die Tiefbohrung Berndorf 1 in den östlichen Kalkalpen un ihr geologische Rahmen. Mitteilungen der österreichischen Geologischen Gesellschaft 74 (75), 137–165.
Wagner III, B.H., Jackson, M.P.A., 2011. Viscous flow during salt welding. Tectonophysics 510, 309–326. https://doi.org/10.1016/j.tecto.2011.07.012.
Waltham, D., 1997. Why does salt start to move? Tectonophysics 282, 117–128.
Warren, J.K., 2016. Evaporites a Geological Compendium Second Edition. Springer. https://doi.org/10.1007/978-3-319-13512-0.
Warsitzka, M., Kley, J., Kukowski, N., 2013. Salt diapirism driven by differential loading – some insights from analog modeling. Tectonophysics 591, 83–97.
Weijermars, R., Schmeling, H., 1986. Scaling of Newtonian and non-Newtonian fluid dynamics without inertia for quantitative modelling of rock flow due to gravity. Phys. Earth Planet. Inter. 43 (4), 316–330.
Weijermars, R., Jackson, M.P.A., Vendeville, B.C., 1993. Rheological and tectonic modeling of salt provinces. Tectonophysics 217, 143–174.